ULTRASONIC ELASTOGRAPHY MEASUREMENTS OF THE MECHANICAL PROPERTIES OF PORCINE CORONARY VESSEL WALLS

A Thesis
Presented to
The Academic Faculty

By

Veerdhaval V. Mahajan

In Partial Fulfillment
Of the Requirements for the Degree
Master of Science in
Bioengineering

Georgia Institute of Technology

August 2005

ULTRASONIC ELASTOGRAPHY MEASUREMENTS OF THE MECHANICAL PROPERTIES OF PORCINE CORONARY VESSEL WALLS

Approved by:

`

Dr. Paul J. Benkeser, Chair
School of Biomedical Engineering
Georgia Institute of Technology

Dr. Arthur Koblasz
School of Electrical and Computer Engineering
Georgia Institute of Technology

Dr. John Oshinski
School of Medicine, *Emory University*
School of Biomedical Engineering, *Georgia Institute of Technology*

Date Approved: July 13, 2005

ACKNOWLEDGMENTS

First and foremost, I would like to thank my advisor, Dr. Paul J. Benkeser for providing me an opportunity to pursue research in an interesting area and his counsel through out. I would also like to thank Dr. Arthur Koblasz and Dr. John Oshinksi for being a part of my thesis committee.

Here at Georgia Tech, I would like to thank Dr. Raymond Vito for his guidance. Lori, Melissa, Peter and Brian from Vito lab for their kind help. Dr. Guldberg and lab, thank you for letting me use the mechanical testing facility. Tracey Couse, thank you for doing everything that you could do to make my research successful. To Dr. Y's lab, Dr. Ku's lab and Daniel thank you for helping me bring those innumerable porcine hearts. Thank you Mr. Hollifield and Hollifield Farms for letting me use the porcine hearts, an integral part of my research.

I thank the administrative staff of Biomedical Engineering, Bioengineering and Petit Institute of Biosciences. A special mention of Chris Ruffin and Pat Fowler for welcoming me into Tech and helping me fill those numerous forms. Tushar, Deepak, Hemir, Varad, Krishna, Lori, Neil, Abhijit, Danli, Binjian, Shayan, Zubair, Shridhar, Rohit my life in Atlanta wouldn't have been same if it wasn't for you all. Ruchira, Kaustubh, Gokul, Manjiri and Vaishali thank you for being there for me when I needed you guys. Rajkumar, Radhika, Kisalay, Rahul, Ronak, Sumit, Milind, Vinayak thank you for always being there for me. I am grateful for having many wonderful people in my life, my friends, my relatives and my grandparents for making my world a better place.

I would like to dedicate this thesis to my parents and my brother for their support, encouragement and great love throughout my life.

TABLE OF CONTENTS

ACKNOWLEDGEMENT……..iii

LIST OF TABLES……vii

LIST OF FIGURES……..viii

LIST OF SYMBOLS……...x

SUMMARY……xi

CHAPTER

1 INTRODUCTION……...1

Atherosclerosis……1

Progression of Atherosclerosis……3

Coronary Arteries……6

Ultrasound……8

Hi-Frequency Application of Ultrasound……..11

Elastography……..12

Principles of Elastography……14

Theory of Elastography……..15

2 METHODOLOGY……..…….18

Transducer……..19

Pulser Receiver……..19

Digitalization and Data Acquisition……...20

Configuration……20

Organ Culture System……22

Automated Control…….23

Specimen Acquisition……23

Data Acquisition……27

System Artifacts…….27

Image Acquisition……..32

3 RESULTS……..33

Data Processing for B-mode image formation……...33

Compression Modulus of fresh porcine coronary artery……...34

Compression modulus of fixed porcine coronary arteries…….35

4 MECHANICAL TESTING……...38

Introduction……38

Procedure……...39

Results……43

5 DISCUSSION……47

Statistical Significance……...47

Conclusion…….48

APPENDIX A: Valpey Fisher VF 412 Transducer. Reflection from glass surface..……49

APPENDIX B: Algorithm for Strain Estimation of pressurized RF waveforms…….….50

APPENDIX C: MATLAB Code for strain computation from pre and post compression RF Waveforms……...51

APPENDIX D: MATLAB Code for Image Formation……..……...54

APPENDIX E: Statistical Tests…….55

REFERENCES……..56

LIST OF TABLES

Table 1: Specifications of Pulser/Receiver (PR 5900, Panametrics Inc) used to acquire data…….27

Table 2: Value of strain and compression modulus of fresh porcine right coronary artery using elastography using elastography …….35

Table 3: Value of strain and compression modulus of porcine right coronary artery fixed with 2% Glutaraldehyde for 30-35 minutes using elastography ……..……36

Table 4: Value of strain and compression modulus of porcine right coronary artery fixed with 3% Glutaraldehyde for 50-55 minutes using elastography.……...36

Table 5: Comparison of effect of Glutaraldehyde on properties of porcine coronary artery measured using elastography.…… ……...37

Table 6: Mechanical testing of fresh porcine coronary arteries using mechanical testing…….44

Table 7: Mechanical testing of fresh porcine coronary arteries fixed by 2% Glutaraldehyde solution for 30-35 minutes using mechanical testing……...44

Table 8: Mechanical testing of fresh porcine coronary arteries fixed by 3% Glutaraldehyde solution for 50-55 minutes using mechanical testing……...44

Table 9: Comparison of effect of Glutaraldehyde on properties of porcine coronary artery measured using mechanical testing……45

LIST OF FIGURES

Figure 1**:** Developmental process of atherosclerosis. [Medical Encyclopedia: U.S. National Library of Medicine]. The development of arterial atherosclerosis may occur when deposits of cholesterol and plaque accumulate at a tear in the inner lining of an artery. As the deposits harden and occlude the arterial lumen, blood flow to distant tissues decreases and a clot may become lodged, completely blocking the artery. http://www.nlm.nih.gov/medlineplus/ency/imagepages/18020.htm ……..2

Figure 2: Normal coronary arterial vessel wall. (Silverthorn DU, Human Physiology: An integrated approach. 2 edition. Prentice Hall)…….3

Figure 3: Fatty Streak: Precursor to Atherosclerotic plaque (Silverthorn DU, Human Physiology: An integrated approach. 2 edition. Prentice Hall…….4

Figure 4: Stable Plaque: Precursor to Atherosclerotic plaque (Silverthorn DU, Human Physiology: An integrated approach. 2 edition. Prentice Hall)……...5

Figure 5: Vulnerable plaque (Silverthorn DU, Human Physiology: An integrated approach. 2 edition. Prentice Hall)……..5

Figure 6: Figure 6: Movat-stained histological section of a non-obstructive human coronary lesion, showing lumen, necrotic core (lipid pool), and fibrous cap. Applied Radiology 30(11): 46-53, 2001……..6

Figure 7: Right and left coronary arteries. [Medical Encyclopedia: U.S. National Library of Medicine]
http://www.nlm.nih.gov/medlineplus/ency/presentations/100160_1.htm……...7

Figure 8: The processes used to generate a ultrasound B-scan. B-scans are composed of a set of axial RF signals representing the response magnitude from a pulse generator using a linear array transducer. Since the response magnitude delays exponentially with depth, it is log-amplified prior to quantization and display……...……...10

Figure 9: Measurement of strain in a one-dimensional cascaded system of unequal spring constants. a) Pre-compression state b) Post-compression state. Observe that the strain in the softer springs depends on the presence of the stiff spring. Ultrasonic Imaging 13, 111-134 (1991)……..15

Figure 10: Components in Ultrasonic Acquisition System……18

Figure 11: VF 412 Valpey Fisher Immersion Style transducer…….19

Figure 12: Pulse Echo Mode……...……...22

Figure 13: Organ Culture System……..23

Figure 14 Fresh Porcine Heart (Hollifield Farms; Covington, GA)……..24

Figure 15: Incision made near junction of Right Coronary Artery and Aorta of a fresh porcine heart to harvest coronary artery……25

Figure 16: Harvesting of RCA from porcine hearts……...25

Figure 17: Porcine Right Coronary Artery tied onto cannulae inside the organ culture setup……...26

Figure 18: Acquired 1-dimensional signal from porcine coronary artery at 80mmHg. Note the baseline noise……...28

Figure 19: Baseline noise of the setup with no target……29

Figure 20: Ultrasound signal of porcine coronary artery with baseline noise subtracted at 80mmHg……30

Figure 21: Ultrasound signal of porcine coronary artery with baseline noise subtracted at 100mmHg..……30

Figure 22: RF Data acquisition by rotating coronary artery in organ culture system……32

Figure 23: 50- MHz ultrasound B-mode image of the proximal wall of a porcine coronary artery……..34

Figure 24: Young's modulus of porcine vessel walls measured by elastography…….37

Figure 25: Uniaxial testing of ring specimens……...38

Figure 26: Biaxial testing of planar surface……...38

Figure 27: Illustration of mechanical ring testing of porcine right coronary artery……..41

Figure 28: 650R Mechanical testing software (Test Resources, MN)……...42

Figure 29: Young's modulus of porcine vessel walls measured by mechanical testing…45

Figure 30: Comparison of Young's modulus of porcine vessel walls measured by elastography and mechanical testing…….46

LIST OF SYMBOLS

R_{lat}	Lateral resolution
R_{ax}	Axial resolution
DOF	Depth of field
λ	Average wavelength
c	Speed of sound
BW	Bandwidth at the transducer
f-number	Ratio of focal length to the diameter of the transducer
σ	Stress
E	Compression modulus
ε	Strain

SUMMARY

Coronary heart diseases are a significant cause of death among both men and women in the industrialized world; thus finding ways to detect factors, which cause coronary heart diseases, is a worthy challenge for researchers. Ultrasound elastography system (50MHz) for measuring mechanical properties of arteries was developed as part of this thesis. Ability to discriminate between various tissue types was demonstrated using fresh and modified porcine coronary arteries, which closely models the plaque in human atherosclerosis. Elastographic measurements agreed well with uniaxial mechanical testing over a range of compression moduli.

CHAPTER 1

INTRODUCTION

Atherosclerosis

Atherosclerosis is a progressive disease characterized by accumulation of lipids and fibrous elements in arteries [1]. From basic cell biology, macrophages (Greek: "big eaters") are cells found in tissues that are responsible for phagocytosis of pathogens, dead cells and cellular debris [2]. Macrophages are part of the innate immune system. Lipid laden macrophages are called foam cells. White blood cells that are produced in the bone marrow but mature in the thymus are called T lymphocytes or T-cells [2]. They are important in the body's defense against certain bacteria and fungi, aiding in making antibodies, and helping in the recognition and rejection of foreign tissues. The early lesions of atherosclerosis consist of sub-endothelial accumulations of cholesterol-engorged macrophages, called foam cells and T lymphocytes. In humans such lesions, called fatty streaks can usually be found in the aorta in the first decade of life, the coronary arteries in the second decade, and the cerebral arteries in the third or fourth decades [1]. Because of differences in blood flow dynamics, there are preferred sites of lesion formation within the branches and bifurcations of arteries [3]. Fatty streaks are not clinically significant, but they are the precursors of more advanced lesions characterized by the accumulation of lipid-rich necrotic debris and smooth muscle cells. Such fibrous lesions typically have a fibrous cap consisting of smooth muscle cells and extra cellular matrix that encloses a lipid-rich necrotic core. Once a fibrous plaque is formed, the process is generally believed to be non-reversible [4]. Although advanced lesions can

grow sufficiently large and eventually block blood flow (Figure 1), the most important clinical complication is an acute occlusion due to the formation of a thrombus or blood clot, resulting in myocardial infarction [1] or stroke [5]. Usually, the thrombosis is associated with rupture of the lesion [1].

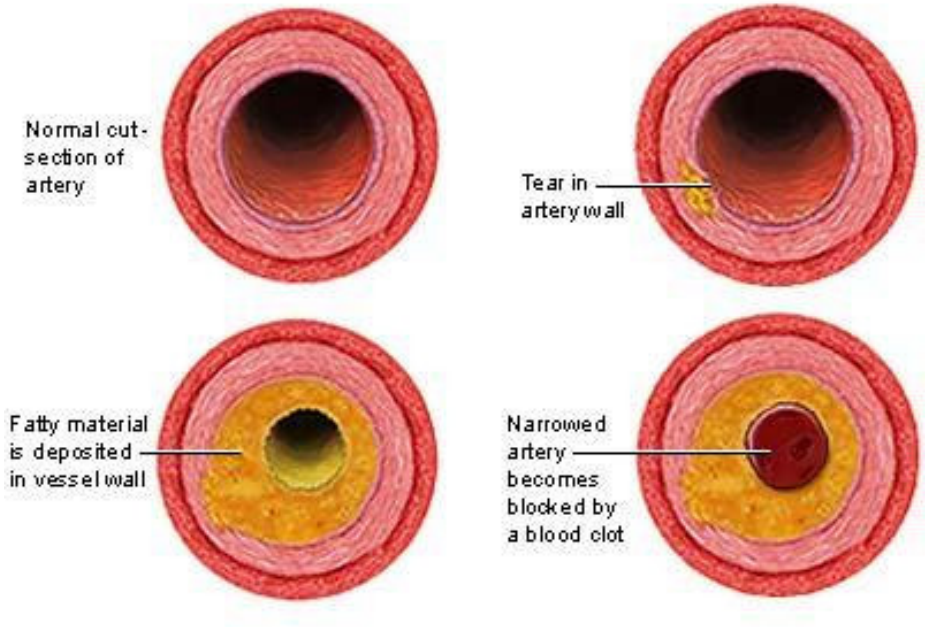

Figure 1: Developmental process of atherosclerosis. [Medical Encyclopedia: U.S. National Library of Medicine]

Plaque rupture is the initiating event in most acute coronary syndromes [1]. Morphological observations at autopsy have identified specific plaque types prone to rupture; commonly referred to in the literature as 'vulnerable plaques' [6]. These plaques are thin-cap fibroatheroma with enclosed fats [7]. The proper identification and treatment of the thin-cap fibroatheroma would have a tremendous impact on the morbidity and mortality from acute cardiac events [6]. The size of the lipid pool within the atherosclerotic plaque and the thickness of the overlying fibrous cap are important

characteristics for predicting the stability of advanced plaques [7]. Vulnerable plaques are characterized by a large lipid pool with a thin fibrous cap [6,7,8]. The shoulder area at the margin of the plaque is a location of high stress, predisposed to rupture [8]. The pathophysiological and clinical significance of lesions is related to plaque size and morphology, and thus plaque stability [8]. Chronic lesions with severe obstruction reduce blood flow and cause stable angina pectoris. However, most acute coronary syndromes are caused by sudden changes of mildly stenotic, vulnerable plaques. The initiating event is rupture or erosion of the fibrous cap, followed by luminal thrombus formation. A major finding in literature in last few years has been that plaque composition, rather the severity of stenosis may determine the risk of thrombotic complication associated with atherosclerosis [6,7,8].

Progression of Atherosclerosis

The normal arterial wall consists of smooth muscle and connective tissue with a layer of endothelial cells lining the lumen of the artery (Figure 2).

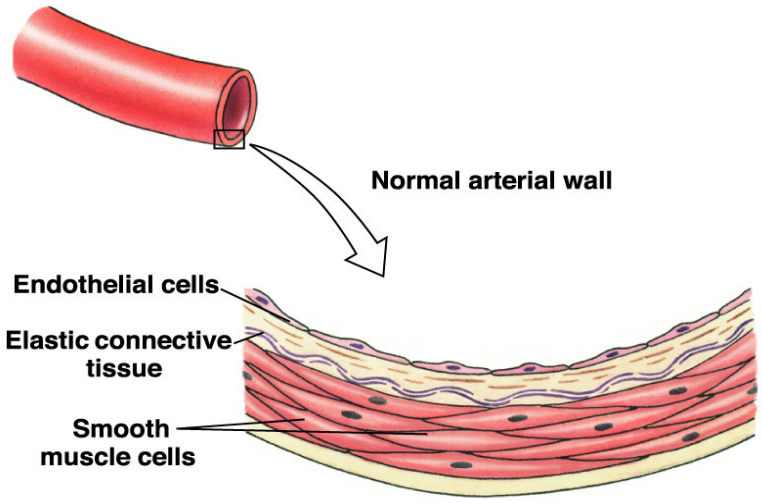

Figure 2: Normal coronary arterial vessel wall. (Silverthorn DU, Human Physiology: An integrated approach. 2 edition. Prentice Hall)

In early stages, excess Low Density Lipoprotein - cholesterol accumulates in the acellular layer between the endothelium and the connective tissue. There, it is oxidized and phagocytosed by macrophages. When the macrophages begin to fill with oxidized cholesterol, they produce paracines, a kind of hormone, that attract smooth muscle cells to that region. At this stage, the lesion is called fatty streak [1,2] (Figure 3).

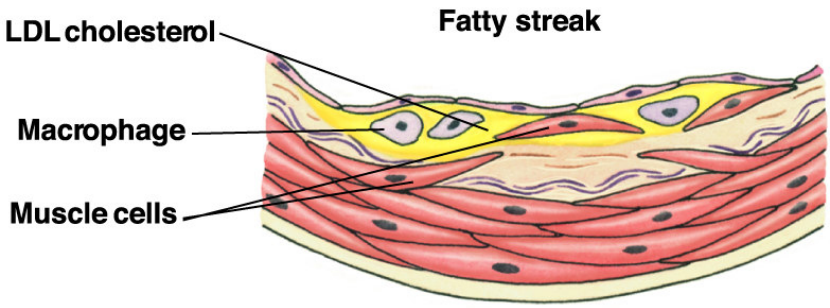

Figure 3: Fatty Streak: Precursor to Atherosclerotic plaque (Silverthorn DU, Human Physiology: An integrated approach. 2 edition. Prentice Hall)

As cholesterol continues to accumulate, fibrous scar tissue forms around it. In addition, the migrating smooth muscle cells divide thickening the arterial wall and narrowing the lumen of the artery [2] (Figure 1, 4).

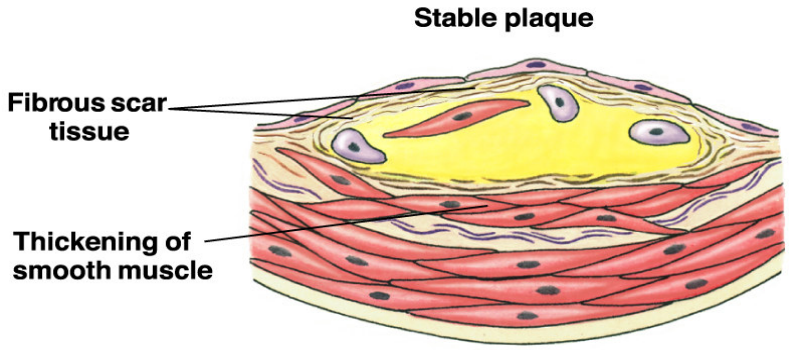

Figure 4: Stable Plaque: Precursor to Atherosclerotic plaque (Silverthorn DU, Human Physiology: An integrated approach. 2 edition. Prentice Hall)

In the advanced stage of atherosclerosis, cells in the fatty deposit may die, and calcified scar tissue will form. This phenomenon causes what is known as "vulnerable plaque", a thin cap fibroatheroma [1,2,6,7,8] (Figures 5-6).

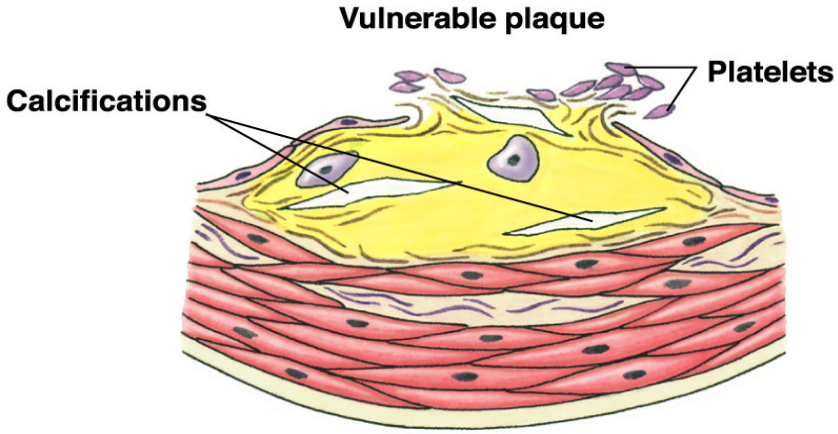

Figure 5: Vulnerable plaque (Silverthorn DU, Human Physiology: An integrated approach. 2 edition. Prentice Hall)

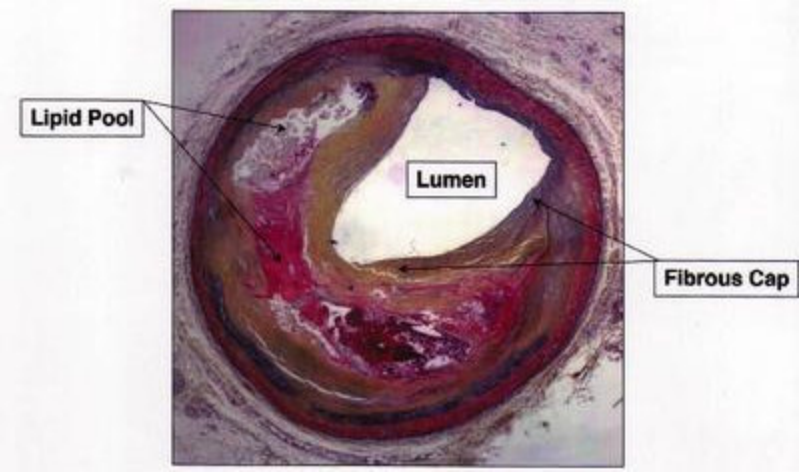

Figure 6: Movat-stained histological section of a non-obstructive human coronary lesion, showing lumen, necrotic core (lipid pool), and fibrous cap.
Applied Radiology 30(11): 46-53, 2001

Coronary Arteries

The coronary arteries are a small part of the arterial tree, but they make up a large percentage of the vessels affected by atherosclerosis. Problems occur when blood flow is compromised due to accumulated plaque and thrombus formation. Partial occlusion of coronary vessels can cause chest pains and near-to-total occlusion causes a myocardial infarction (heart attack).

Because coronary heart diseases are such a significant cause of death among both men and women in the industrialized world, thus understanding coronary arteries and the factors that lead to the diseased state is a worthy challenge for researchers. The role of the coronaries is to perfuse the heart with oxygenated blood. The coronaries are located between the epicardial and myocardial layers of the heart, often embedded in fat.

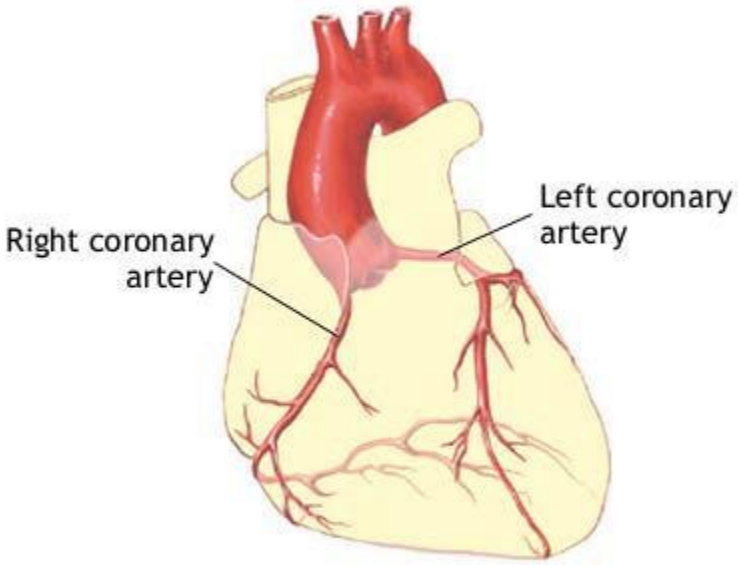

Figure 7: Right and left coronary arteries. [Medical Encyclopedia: U.S. National Library of Medicine]

The coronaries begin as two main vessels branching off the aorta just above the aortic valve (Figure 7). The primary branches are the right coronary artery (RCA) and the left main. The left main further branches into the left anterior descending and left circumflex. When functioning properly, the coronaries supply blood to many areas of the heart muscle. Regulation of the coronary arteries is by physical, metabolic and neural means. Coronary artery smooth muscle cells are controlled by the metabolism to balance supply of blood with demand. This is accomplished by physical changes in diameter, which influence the flow and the pressure. Approximately 60% of all human deaths are caused by disorders of the cardiovascular system [9]. A blood vessel can be divided anatomically into three distinct cylindrical sections when viewed under a microscope (Figure 2).

These structures have distinct functions in terms of blood vessel physiology and mechanical properties. The intima consists of a thin monolayer of endothelial cells that line the inner surface of the vessel. The endothelial cells have little influence on blood

vessel mechanics but do play an important role in hemodynamics and transport phenomena [9]. The media represents the major portion of the vessel wall and provides most of the mechanical strength necessary to sustain structural integrity [2]. The media is organized into alternating layers of interconnected smooth muscle cells and elastic lamellae. The elastic lamellae are composed principally of the fibrous protein elastin. The number of elastic lamellae depends upon the wall thickness and the anatomical location of the vessel. The adventia consists of loose disorganized fibrous connective collagen, fibroblasts, nerves and vasa vasera and has less influence on mechanics than media. Under normal conditions, arteries have nonlinear pressure-radius relations at lower pressure ranges; the diameter greatly increasing with pressure (below 60mmHg). However at higher pressures, the diameter change is less severe [2].

Ultrasound

The use of ultrasound in the modern-day medical clinic has found a solid niche among the various methods for imaging the body. Ultrasound is defined as acoustic waves with frequencies above those that can be detected by the ear, from about 20 kHz to several hundred MHz [10]. Medical ultrasound typically uses only the portion of the ultrasound spectrum between 1 MHz and 10 MHz due to the tradeoff between frequency and depth of penetration. The waves are generated by small acoustic transducers, which that are electrically driven and typically placed on the skin. The waves propagate into the tissue of the body where a portion is reflected from the myriad of interfaces between tissues with different acoustic properties [10].

The most commonly used modality in medical ultrasound is B-mode imaging, where an ultrasound transducer is placed against the skin directly over the region of interest (ROI).

A typical ultrasound transducer employs an array of piezoelectric elements to generate short in duration, broadband pulses (with a center frequency of about 3-15MHz). The array size determines the imaging system's aperture. The same transducer also receives the backscattered signals. The transmit signals passing to and the received signals passing from the array elements can be individually delayed in time, defining a phased array. Phased arrays are used to electronically steer and focus the sequence of acoustic pulses through the target volume which is know as beam forming. Processing these echo signals routinely begins at the individual channel (element) level to produce A-lines (A-mode/ one dimensional wave equation of sound energy reflected from the target). The general formation of B-mode sequences (Figure 4) commences with RF demodulation or envelope detection storing resulting A-modes in a 2D image matrix, followed by attenuation correction using time gain compensation (TGC) or swept and lateral gains to increase signal amplification from increasing depths. Next scan conversion (a 8 bit digitization) allows the B-mode to be displayed with a defined resolution (known as a B-scan), and finally logarithmic compression is used to adjust the large echo dynamic range (60-100 dB). The B-scan sequences captured and analyzed are those processed and displayed by the ultrasound machine, with a uniform dynamic range of intensities between 0 and 255[9].

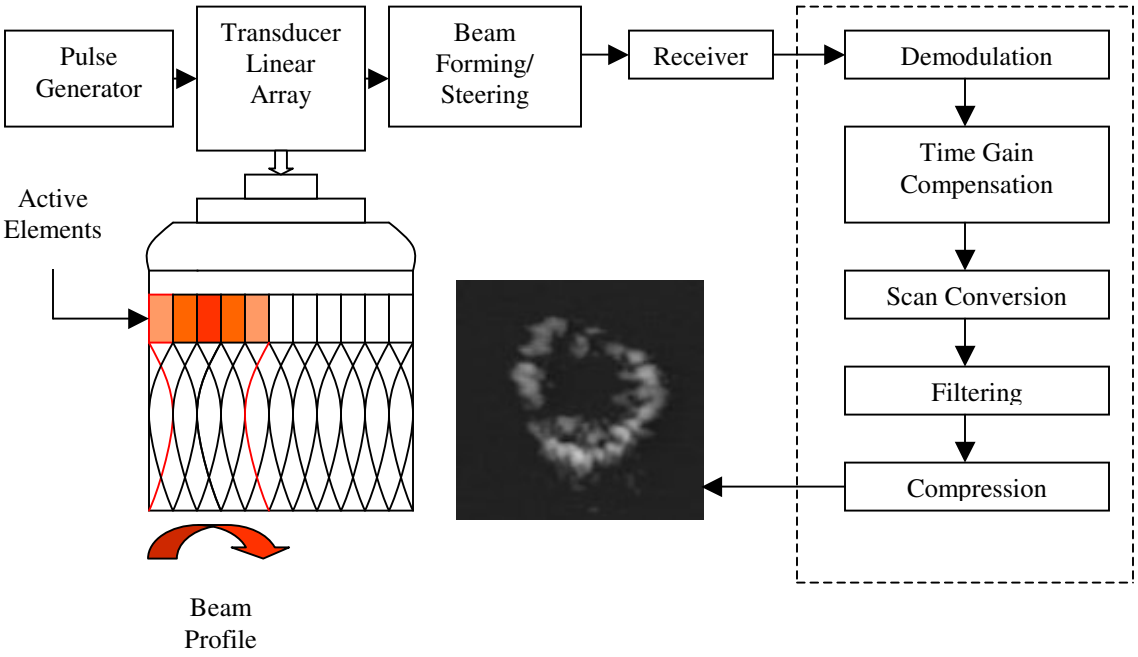

Figure 8: The processes used to generate a B-scan. B-scans are composed of a set of axial RF signals representing the response magnitude from a pulse generator using a linear array transducer. Since the response magnitude delays exponentially with depth, it is log-amplified prior to quantization and display. *(Ultrasonic Bioinstrumentation* John Wiley & Sons 1998)

Speckle Formation

Ultrasound image analysis in general is complex due to numerous tissue interfaces and varying structure of biological tissues causing echogenecity, which is described in terms of speckle formation. Speckle is structured noise from a medium containing many scatterers. Speckle appearance is dependent on bandwidth, frequency and manufacturer of the employed transducer, in addition to the geometry and sub-wavelength structure of the tissue. Echographic speckle texture of imaged tissue is mainly due to intensity scattering; implying structures are smaller than the sampling volume (a product of spatial pulse length and beam cross section). Upon visual inspection speckle consists of a

relatively high grey level intensity, qualitatively ranging between a hyperechoic (bright) and hypoechoic (dark) domain. Scatter occurs when small imperfections (scatterers) in the target cause seemingly random reflections and refractions of the sound wave. The textures created do not correspond to underlying structure, but the intensity reflects the local echogenecity of the underlying scatterers. Scatterers account for a decrease in image quality, causing blurring and decreased intensity at impedance boundaries, while within the medium they create speckle. The statistics of the signal depends on the density of scatterers, with a large number of randomly located scatterers following a Rayleigh distribution (known as fully developed speckle) [10].

Hi-Frequency Application of Ultrasound

As in ultrasound imaging in the diagnostic frequency range, the choice of system design specifications depends on the nature of the application and the acoustic properties of the specific tissues being imaged. The ultimate imaging performance of any ultrasound system is determined by the frequency, geometry of the transducer and tissue properties. These issues were discussed by Foster et.al. [11], who described the tradeoffs between resolution, penetration and system dynamic range. The quality of the image is determined by the beam distribution (lateral resolution R_{lat}) and the pulse bandwidth (axial resolution, R_{ax}). Simplified expressions for lateral resolution, $R_{lat,}$ axial resolution, R_{ax} and depth of field, DOF, for a spherical radiator at the focus are [5]:

$$R_{lat} = \lambda \left(\frac{\text{focal length}}{\text{diamater}} \right) = \lambda \text{ (f-number)} \qquad (1)$$

$$R_{ax} = \frac{1}{2} \frac{c}{BW} \qquad (2)$$

$$\text{Depth of Field} = 7.0\,\lambda\,(\text{f-number})^2 \qquad (3)$$

where λ is the average wavelength, c is the speed of sound and BW is the bandwidth at the transducer and f-number is the ratio of focal length to the diameter of the transducer. Depending on the choice of frequency and f-number, the resolution can vary over several orders of magnitude. Improvement in transducer frequency and f-number can improve the resolution significantly. However as has been discussed there are problems associated with high frequency arrays. Important issues at higher frequencies are loss of penetration, loss of depth of field, relative change in conspicuity due to changes in the backscatter of ultrasound from blood, and issues related to the manufacturability of transducers.

Elastography

Imaging of the elastic properties of tissues has become the subject of increasing research effort. The goal of elastic imaging is to map tissue properties such as Young's modulus or stiffness to provide useful clinical information. Changes in soft tissue stiffness may be related to an abnormal pathological process; for example, some tumors of the breast, liver and prostate are associated with increases in tissue elasticity caused by increased density. Diseases such as atherosclerosis involve fatty and/or collagenous deposits, which changes tissue elasticity. Physicians have relied on palpation of hard areas in tissue to aid in tumor detection. Present cross-sectional imaging methods display tissue parameters like attenuation (in X-ray), interferences (in ultrasound) or proton density (in MRI) not directly associated with the findings on palpation. Various elastography techniques developed using different modalities (ultrasound, MRI and optics), employ different tissue excitations and extracting different parameters of tissue motion [13,14,15,16]. The

most popular of these techniques is ultrasound, perhaps due to availability of Radio Frequency information of tissue, which represents propagation of sound waves through tissue.

Biological tissues can be modeled as homogeneous gels. Different modes of propagation of elastic waves in such media are determined primarily by their bulk (K) and shear (G) elastic moduli. In biological soft tissues $K >> G$. The bulk properties (and hence the ultrasonic properties) are determined primarily by the molecular composition of the tissue, while the higher level of tissue organization determines shear properties. Since deformable soft tissues are essentially volume-incompressible (i.e. their Poisson's ratio ~ 0.5), their shear moduli are proportional to their longitudinal (Young's) moduli [17]. It follows that estimation and imaging of the Young's moduli of tissue should in principle convey information about their shear properties, and hence the higher level of tissue organization [17]. Strictly speaking, tissue is inelastic [9]. It does not meet the definition of an elastic material, which requires that there be a single valued relationship between stress and strain. Biological tissues exhibit viscoelastic properties such as hysteresis, stress relaxation, and creep [9]. They are anisotropic and the strain-stress relationship is non-linear. Hence, it is difficult to describe the mechanical properties of tissue without a significant degree of simplification. Tissue models which include series (Maxwell model) and parallel (Voigt model) elastic and viscous components have been described [9]. Such models rely on simplifying assumptions such as considering uniaxial applied stress and linear relationships between forces acting on the tissue and deformations to simplify analysis [9].

Ultrasonic methods for deriving information related to the motion (displacement or velocity) and the elastic moduli of soft tissues have been described in the literature over the past 15 - 20 years [18,19,20,21]. There are various methods used to estimate mechanical properties in the ultrasound domain. These methods identify patterns or features derived from analysis of the ultrasonic signals or images obtained from mechanically perturbed tissues in order to assess their elastic characteristics.

In the early 1990's Ophir and his group described methods for quantitative imaging of strain and elastic modulus distributions in soft tissues [9]. The method is based on external tissue compression with subsequent compression in strain profile along the transducer axis, which is developed from cross-correlation analysis of pre- and post-compression A-line pairs. The strain profile can then be converted to an elastic modulus profile by measuring the applied force.

Principles of Elastography

Consider a system with three springs with same length without any application of force. (Figure 9) Spring constant is defined as the force necessary to stretch (or compress) a spring a unit length. In the considered system, the springs have different spring constants; with the spring in middle having greater spring constant (more rigid) while other two springs having lesser spring constant (less rigid) than the one in middle. On application of equal forces on the springs, the less rigid spring will yield more displacement as compared to the rigid one. The rigid spring is mechanically less elastic; thereby producing less displacement vis-à-vis the less rigid spring, which deforms more due to the same force.

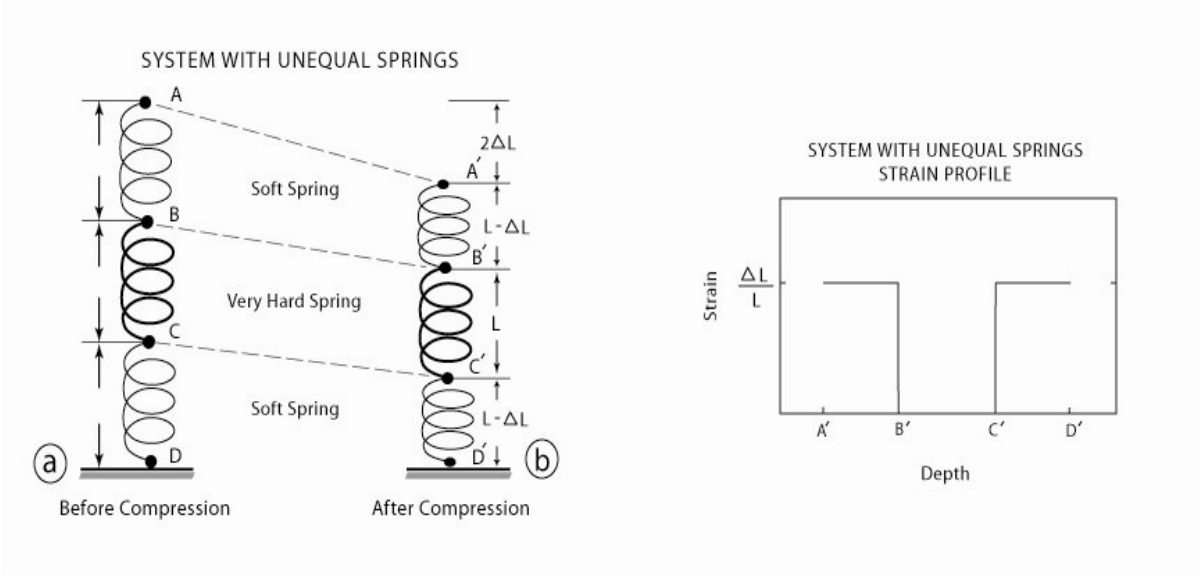

Figure 9: Measurement of strain in a one-dimensional cascaded system of unequal spring constants. a) Pre-compression state b) Post-compression state. Observe that the strain in the softer springs depends on the presence of the stiff spring. Ultrasonic Imaging 13, 111-134 (1991)

Elastography follows analogy of the spring example; tissues in general have varying mechanical properties [9]. When subjected to similar forces, tissues with higher elastic modulus deform less, as compared to tissues with lower elastic moduli. Using cross-correlation function, one can measure such deformation (strain) and with information about the applied force (stress), one can deduce the elastic moduli.

Theory of Elastography:

The stress applied to the tissue is quasi-static. This essentially avoids problems due to reflections, standing waves and mode patterns that may interfere with quality image formation. The applied quasi-static uniaxial stress reduces the complexity of the generalized viscoelastic equation of forced motion of the form

$$M\frac{d^2x}{dt^2} + R\frac{dx}{dt} + Kx = F_o e^{j\omega t} \qquad (4)$$

that contains inertial (M), viscous (R), and stiffness (K) controlled terms, the displacement (x), the force amplitude (F_o), and the angular vibrational frequency, (ω) to the much simpler Hookean equation

$$Kx = F_o \qquad (5)$$

Since $\omega = 0$ and x is a constant, the velocity and acceleration terms vanish. In principle, this allows the isolation and direct extraction of the local tissue stiffness parameter (K) from measurement of differential applied force (or stress) and the resulting local changes in displacement x. Determination of the global stiffness of gels and human muscle in vivo have been reported [11,12]. The average levels of strain evoked in the tissue are very small (on the order of 0.01 or less). These strain levels are considered small enough to keep the Hookean equation well within the linear range, based on the linear strain/stress relationships for gels and human muscle *in vivo* reported by Mridha and Odman [11]. Results with arteries have also been documented in the literature [19,20].

When an elastic medium such as tissue is compressed by a constant uniaxial stress, all points in the medium experience a resulting level of longitudinal strain whose principal components are along the axis of compression. If one or more of the tissue elements has a different stiffness parameter from the others, the level of strain in that element will be higher or lower; a harder tissue element will generally experience less deformation is estimated in one dimension from the analysis of ultrasonic signals obtained from ultrasound equipment. This is accomplished by acquiring a set of digitized radiofrequency echo lines from the tissue and then compressing the tissue with the ultrasonic transducer (or applying mechanical forces like pressure changes in coronary arteries as is done in this thesis) along the ultrasonic radiation axis by a small amount and

acquiring a second, post compression set of RF lines from same region. Congruent echo lines are then subdivided into small temporal regions that are compared pair wise using a cross-correlation technique, from which the changes in time arrival of echoes before and after can be estimated. Because of the small magnitude of the applied compression, there are only small distortions of the echo lines, and the changes in arrival times are also small. The local longitudinal strain $e11,_{local}$ (which in case of coronary artery is along the axial axis) may be estimated as [9];

$$e11,_{local} = \frac{(t1_b - t1_a) - (t2_b - t2_a)}{t1_b - t1_a} \quad (6)$$

where $t1_a$ is the arrival of time of the precompression echo from the proximal window, $t1_b$ is the arrival time of the postcompression echo from the distal window, $t2_a$ is the arrival time of the postcompression echo from the proximal window, and $t2_b$ is the arrival time of the postcompression echo from the distal window. The windows are translated in small overlapping steps along the temporal axis of the echo line and the calculation is repeated for depths.

The two fundamental assumptions made are that [26]

i) One-dimensional deformation is considered for an applied force

ii) Speckle motion adequately represents the underlying motion for small uniaxial compression.

The time delays in equation (5) may be derived by estimating the location of peak of the crosscorrelation function of precompression and post compression echo signals [9], which is used and later described in this thesis.

METHODOLOGY

Hypothesis: Elastography technique at 50 MHz can be used to discriminate between various elastic moduli of coronary vessel.

The ultrasound acquisition consists mainly of the following parts (Figure 10)

Transducer

Pulser/Receiver

Digitalization and Data Acquisition

Recording Device

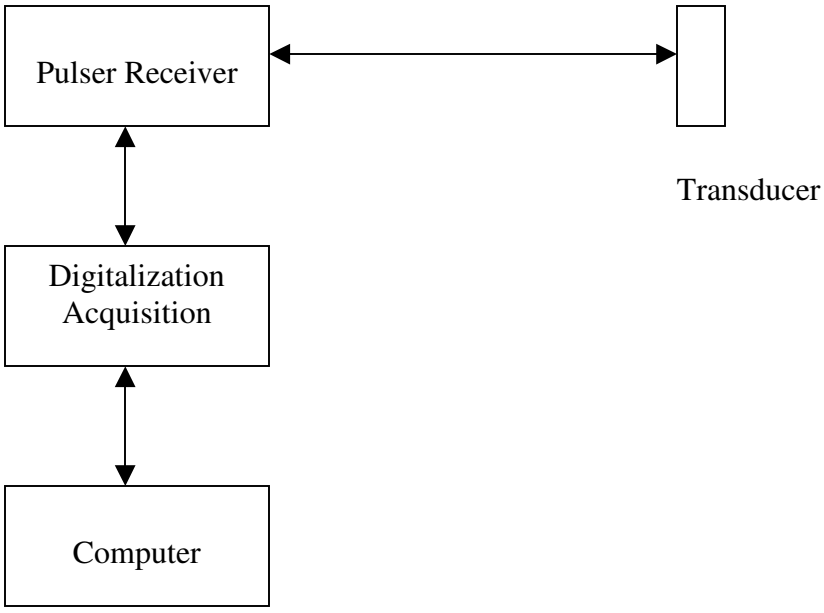

Figure 10: Components in Ultrasonic Acquisition System

Transducer

A Valpey Fisher 50 MHz transducer (VF 412) was used to collect Radio Frequency (RF) data (A-line) (Figure 11). The nominal frequency of the VF 412 is 50 MHz with an element diameter of 5.08 mm and a focal length of 127 mm. A microdot connector connects the transducer to the pulser/receiver system. The transducer has a spherical focus (Figure 11) produced with aid of concave lens. Such a concave structure results in an air-bubble formation when placed in organ culture system, discussed later in this thesis.

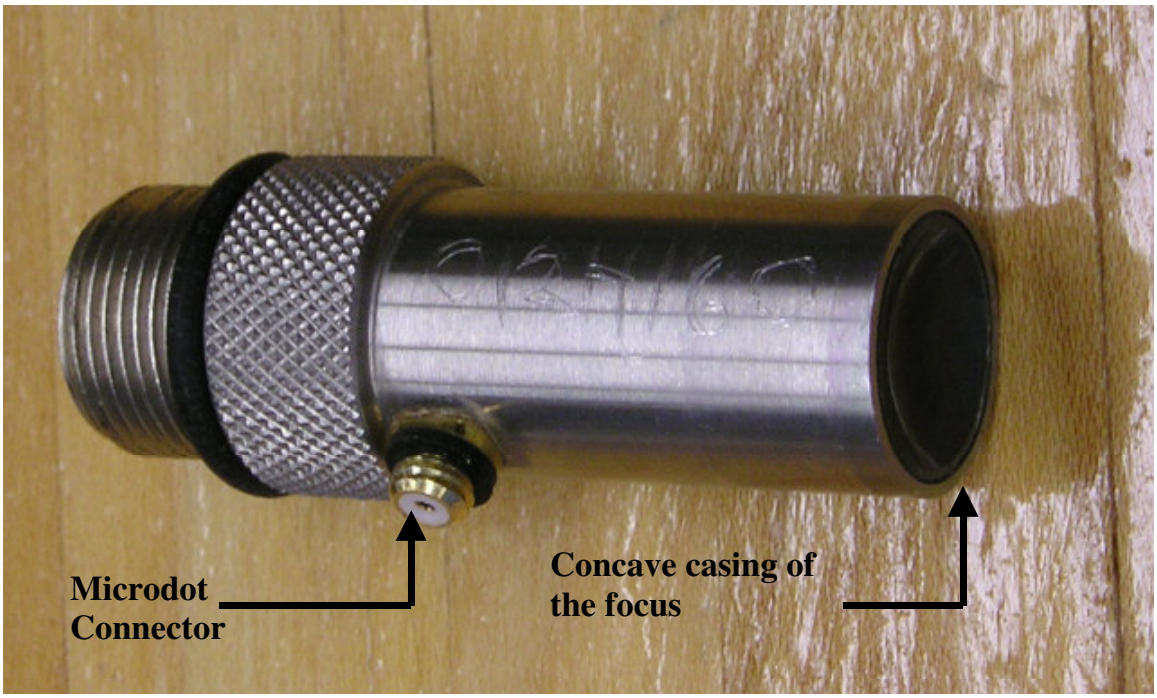

Figure 11: VF 412 Valpey Fisher Immersion Style transducer

Pulser Receiver

Model 5900PR (Panametrics Inc) pulser receiver was chosen due to its high bandwidth (200 MHz) and ability to communicate via an RS –232C port with Labview software.

Digitalization and Data Acquisition

RF signals used to compute time delay estimators are sampled and quantasized. Researchers have used simulated models of uniformly elastic phantoms to find mechanical properties [22]. A study of the dependence of the strain values on the quantization and sampling rates has been performed in scientific literature [22]. The results indicated that the resolution of the strain value improves with both the sampling rate and the quantization. It was recommended that the acquisition sampling frequency be about 4 times the frequency of the transducer frequency.

An Agilent 54642A model oscilloscope was chosen due to its high bandwidth (500 MHz) and high sampling rate of 2 Gsa/sec. Another factor in using the 54642A was its RS232c and GPIB (IEEE 488) interfaces.

Configuration

The pulse-echo method is one of the most commonly used methods/configurations in ultrasound. In the pulse-echo ultrasonic testing technique, an ultrasound transducer generates an ultrasonic pulse and receives its echo (Figure 12). The ultrasonic transducer functions as both a transmitter and receiver in one unit. Most ultrasonic transducer units use an electronic pulse to generate a corresponding sound pulse, using the piezoelectric effect. A short, high voltage electric pulse (less than 20 ns in duration and 100-500 V in amplitude) from the pulser/receiver excites a piezoelectric crystal, to generate an ultrasound pulse. The transducer broadcasts the ultrasonic pulse at the surface of the specimen. The ultrasonic pulse travels through the specimen and reflects off the opposite face. The transducer then listens to the reflected echoes. The ultrasound pulse keeps

bouncing off the opposite faces of the specimen, attenuating with time. The time between any two echoes is the length of time required for the pulse to travel through the specimen and back to the transducer. Speckle is made up of these RF waves. The attenuation (amplitude decay) is exponential with time. The speed of sound in the solids can be derived from the observed round trip transit time, t, and the measured thickness of the specimen, d:

$$c = \frac{2 * d}{t} \tag{7}$$

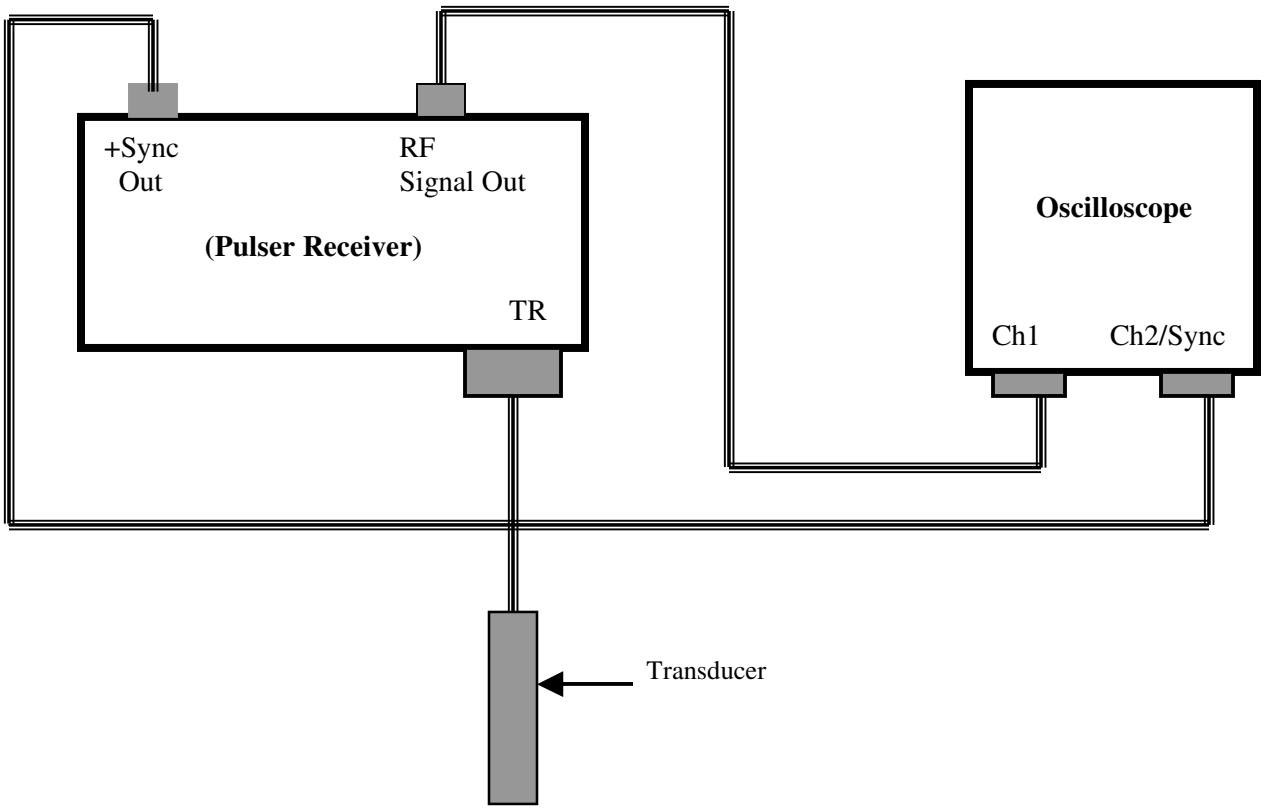

Figure 12: Pulse Echo Mode

Organ Culture System:

A system to pressurize coronary arteries (Figure 13) was developed to acquire ultrasound RF signals at different pressures (80mmHg and 100mmHg). A Plexiglas chamber was constructed which would suspend the coronary artery in a liquid medium. At the center of the two sides of the chamber, provision was made to place cannulae on a gear system, which offered zero back slash and a resolution of ½ degree. The gear system was electronically controlled using Minilab 1008, which is USB based data acquisition device. The output of a Master flex 7520 peristaltic pump was used to develop pressure in the closed system containing the coronary artery. An electronic pressure transducer (Harvard Apparatus, Natick, MA) was used to monitor the pressures.

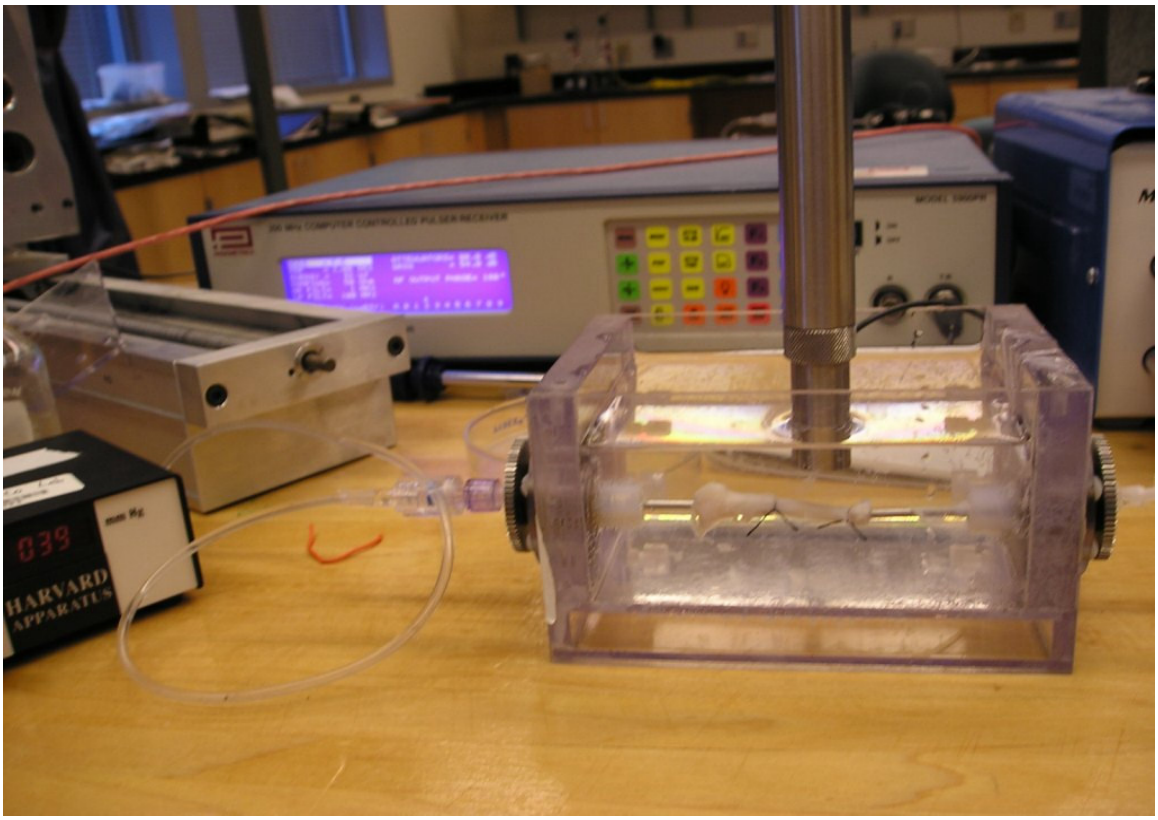

Figure 13: Organ Culture System

Automated Control

The oscilloscope was connected to a Pentium IV computer using the GPIB interface. The Minilab 1008 DAQ was used to control the movements of the artery and automate the pressurization. Automated control was possible using Labview 7.0 software. The control programs are appended at the end of this thesis in Appendix.

Specimen Acquisition

Cardiovascular physiology of domestic pigs is one of the few non-primitive animal models used in cardiovascular research. The physiology and anatomy of porcine hearts is very similar to that of humans [22,23,24]. Porcine hearts were obtained from a local farm (Hollifield Farms, Covington, GA) and carried to Georgia Tech within 2 hours of

sacrifice. The weight of the pigs ranged about 200 - 350 pounds. The hearts were preserved on ice. The right coronary arteries were excised from intact hearts (Figure 14) approximately 3-4 hours after sacrifice. For the excision the right atrium was removed first. Right Coronary Artery (RCA) was used due to its fewer number of branches. The excision of the artery from the heart was started about 10-15 mm from the junction of aorta and RCA (Figure 15). Excess connective tissue on the artery was removed with a scalpel or tissue scissors.

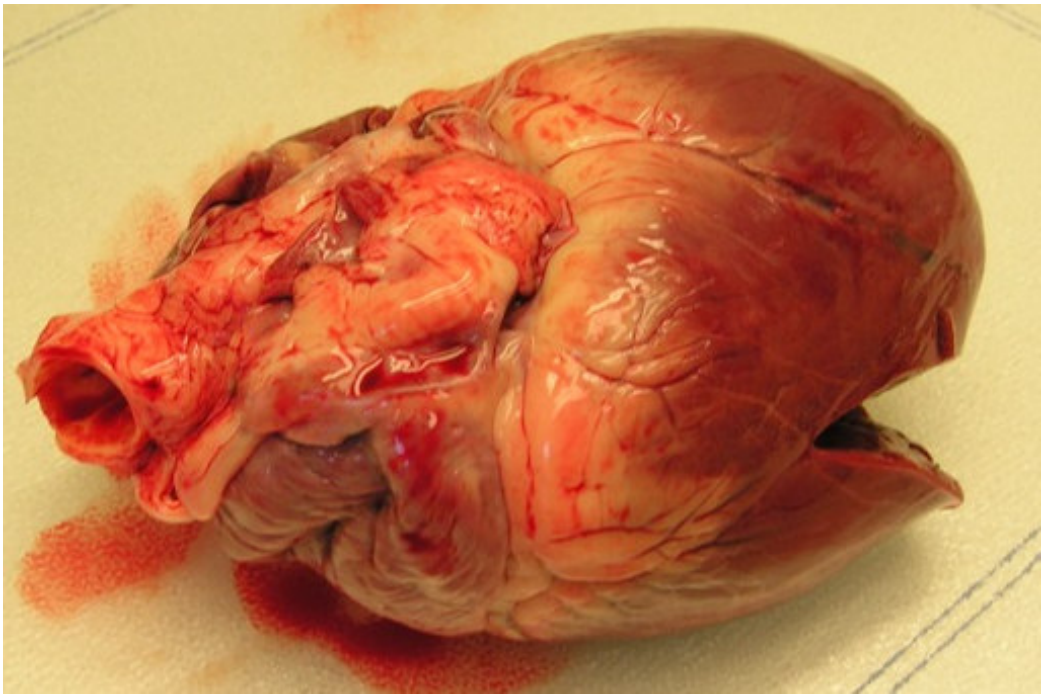

Figure 14 Fresh Porcine Hearts (Hollifield Farms; Covington, GA)

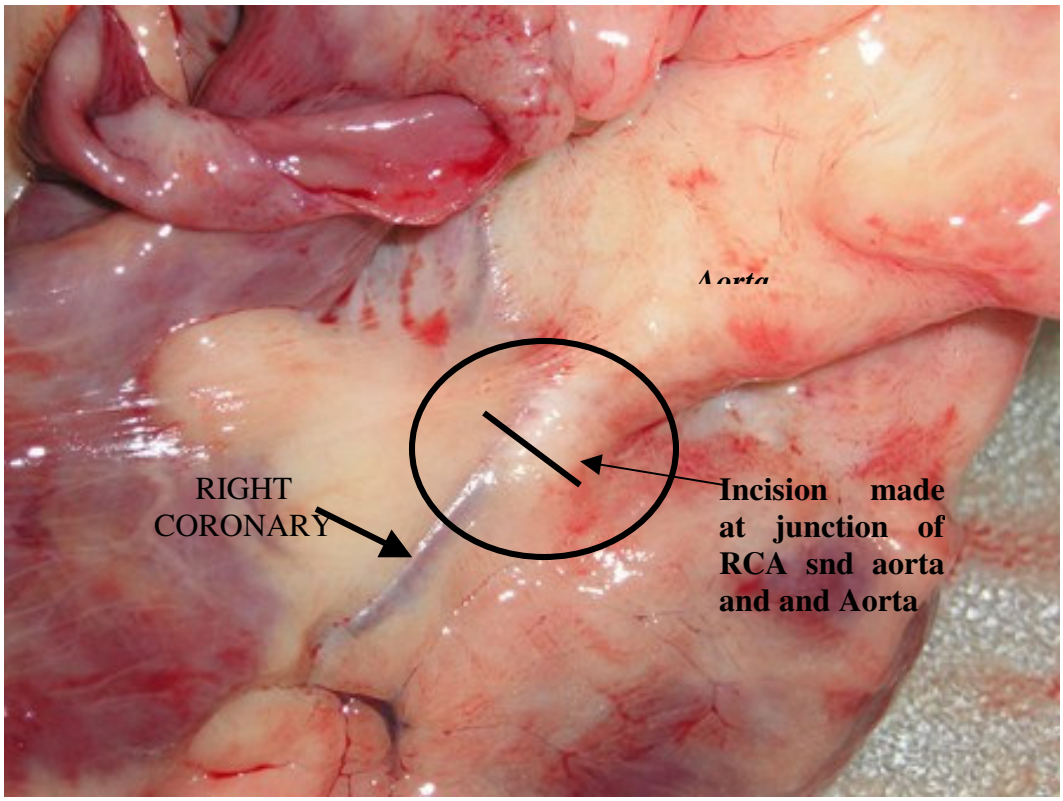

Figure 15: Incision made near junction of Right Coronary Artery and Aorta of a fresh porcine heart to harvest coronary artery

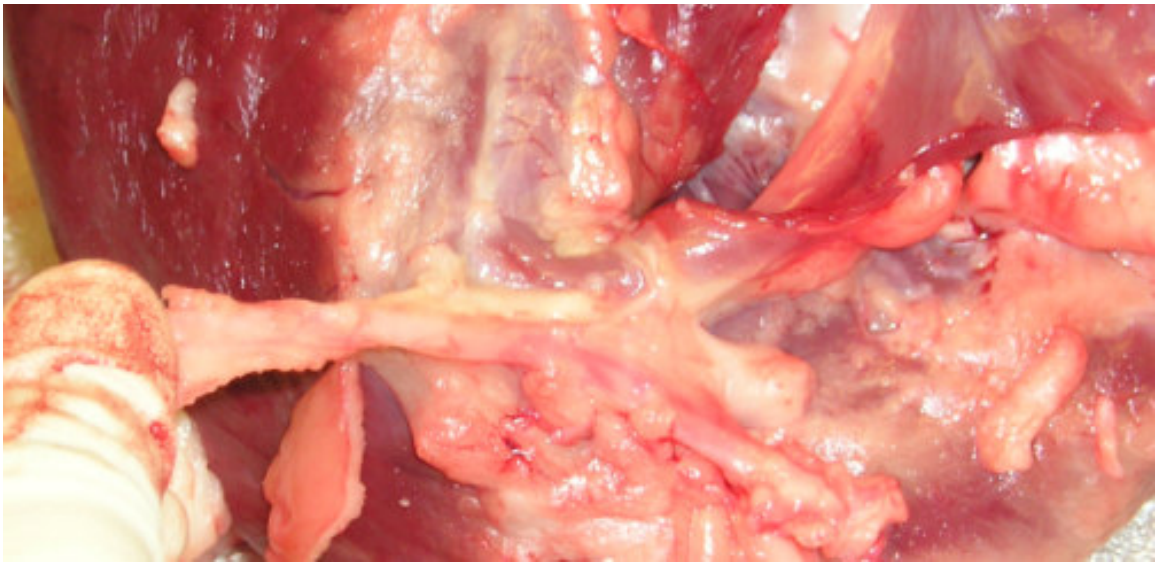

Figure 16: Harvesting of RCA from porcine hearts

It was a challenge to find segments of adequate length (no less than 1.5 cm) with no branches. For this reason, prior to excision, each artery was injected with a mixture of green food color (Kroger Co. brand) and Phosphate Buffered Saline (PBS) (Sigma P3813 Phosphate Buffered Saline, pH 7.4). This allowed branches to be traced and tied off. Only segments with branches less than 25% the size of the artery diameter were used in the testing. This excluded the distal parts of most arteries [20]. Once the specimen was excised, it was placed in container of PBS to remove traces of food coloring and blood.

The excised artery was mounted on the cannulae, which are positioned inside the organ culture system (Figure 17). The cannulae have grooves on them to enable fastening of the arteries without any leakage. Arteries shrink when harvested from hearts due to their release from *in vivo* stretch [9]. While tying the artery onto the cannulae, the artery was stretched by about 1.5 times the original length to keep it close to its normal anatomical conditions [9].

Figure 17: Porcine Right Coronary Artery tied onto cannulae inside the organ culture setup

Data Acquisition

The transducer was positioned above the artery sample, submerged in Phosphate Buffered Solution (PBS) solution. The distance between the face of the transducer and the artery was kept approximately 1.27 cm; the focal length of the transducer. Due to its spherical concave lens, a bubble formation took place when the transducer was placed inside the organ culture system. Care was taken to remove the bubble formation by covering the face of the transducer when submerging it in the organ culture system. Table 1 includes specifications of Pulser/Receiver used to acquire the data.

Table 1: Specifications of Pulser/Receiver (PR 5900, Panametrics Inc) used to acquire data

Mode	**P/E (Pulse Echo)**
PRF (Pulse Repetition Frequency)	200 Hz
Energy	32μJ
Damping	50 ohms
High Pass Filter	1MHz
Low Pass Filter	100MHz
Attenuation	0dB
Gain	54dB

System Artifacts

Hi frequency transducers have buffering to alleviate internal reflections. The buffering in the transducer can produce a random background artifact, which mixes with the actual signal from the target [10]. The frequency of this artifact is in the same range (30 – 50

MHz) as that of ultrasound signals from the target. Hence, after every acquisition a blank acquisition (acquiring data with no target) was recorded. Subtracting the acquired signal with baseline signal eliminated this baseline effect.

Figure 18 and 19 show the RF signals (A-lines) from the porcine coronary artery target and without a target, respectively.

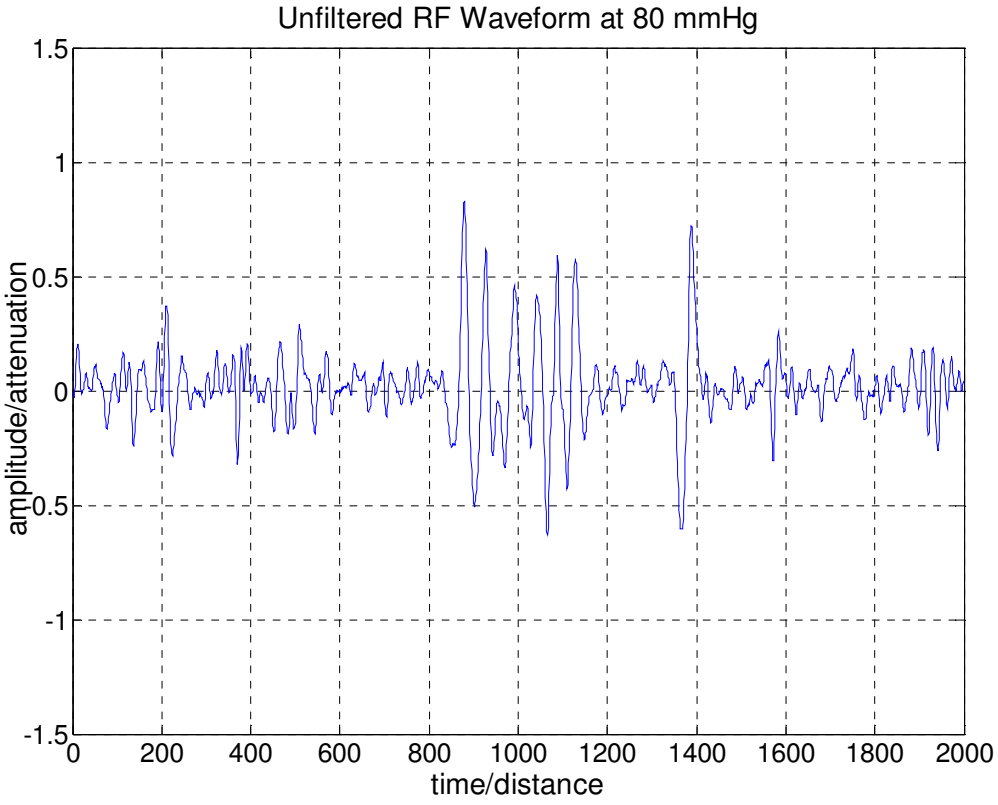

Figure 18: Acquired 1-dimensional signal from porcine coronary artery at 80mmHg. Note the baseline signal

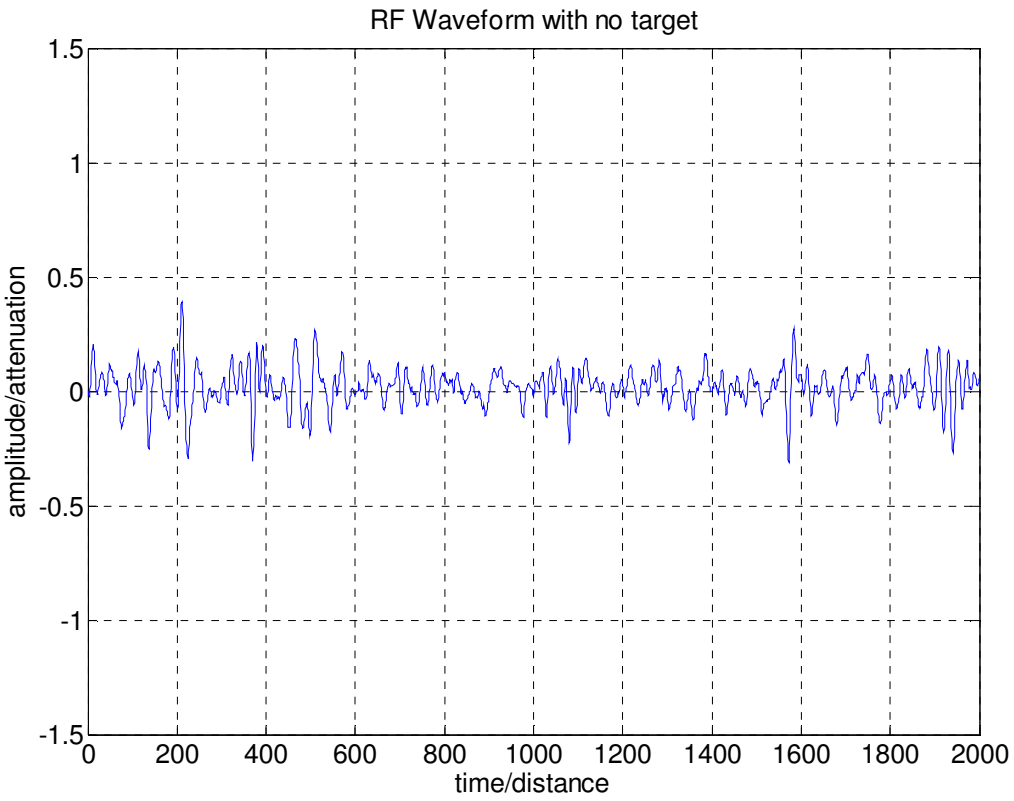

Figure 19: Baseline signal of the setup with no target

Subtracting the baseline signal data (Figure 19) from data acquired with the target yields an RF signal with the baseline signal removed (Figure 20).

For each artery sample 3 sets of RF waveforms were over a cross section of the artery, by rotating the artery about its axis. Each set of signals consists of waveforms at 80mmHg (± 2mmHg) and 100mmHg (± 2mmHg) (Figures 20 and 21). A digital pressure transducer (Harvard Apparatus, Natick, MA) was used to monitor the pressure inside the artery.

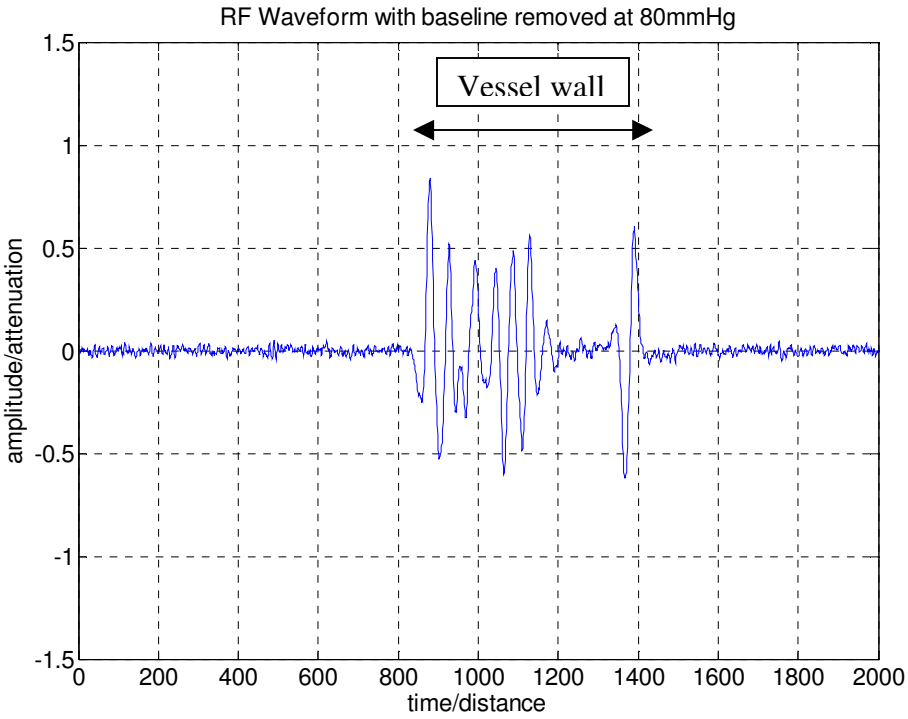

Figure 20: Ultrasound signal from porcine coronary artery with baseline noise subtracted at 80mmHg.

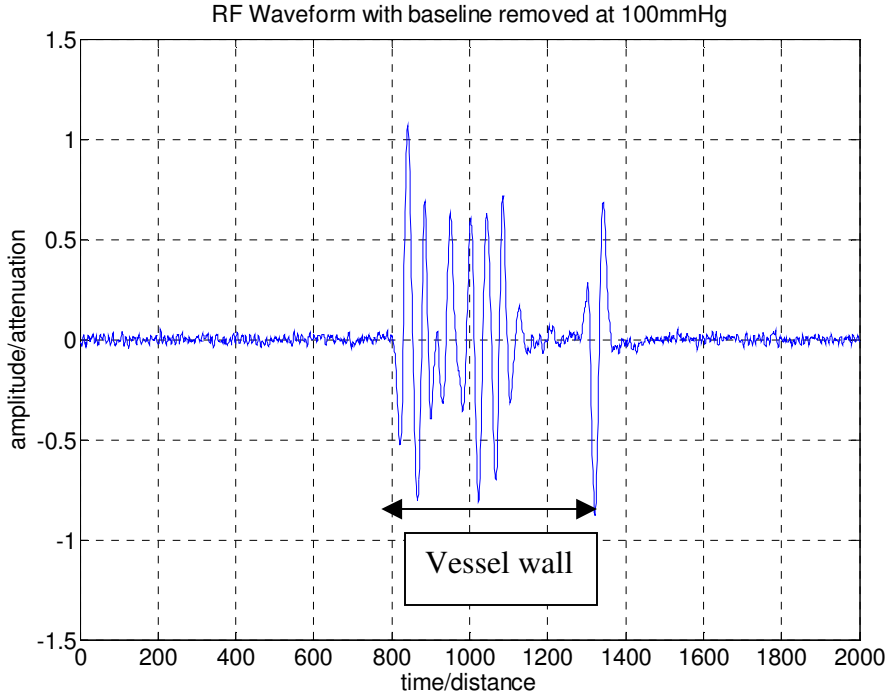

Figure 21: Ultrasound signal from porcine coronary artery with baseline noise subtracted at 100mmHg.

After acquiring ultrasound data from fresh porcine coronary arteries, the organ culture system was then filled with either a 2% Glutaraldehyde solution ($HCO\text{-}(CH_2)_3\text{-}CHO$) for 30-35 minutes or a 3% Glutaraldehyde for 50-55 minutes to effectively change its mechanical properties. Glutaraldehyde, an aldehyde fixative stabilizes the structure of cells and tissues effectively increasing the elastic modulus. Three more sets of readings were taken at 80 and 120mmHg pressures with Glutaraldehyde fixed arteries. Artery rings were cut 5-6mm in width using a razor blade for the mechanical testing discussed later in this thesis.

Image Acquisition

Raw ultrasound RF data was recorded using the 50MHz ultrasound transducer. A total of 100 A-line scans were acquired, which translates to about 90° of artery cross-section.

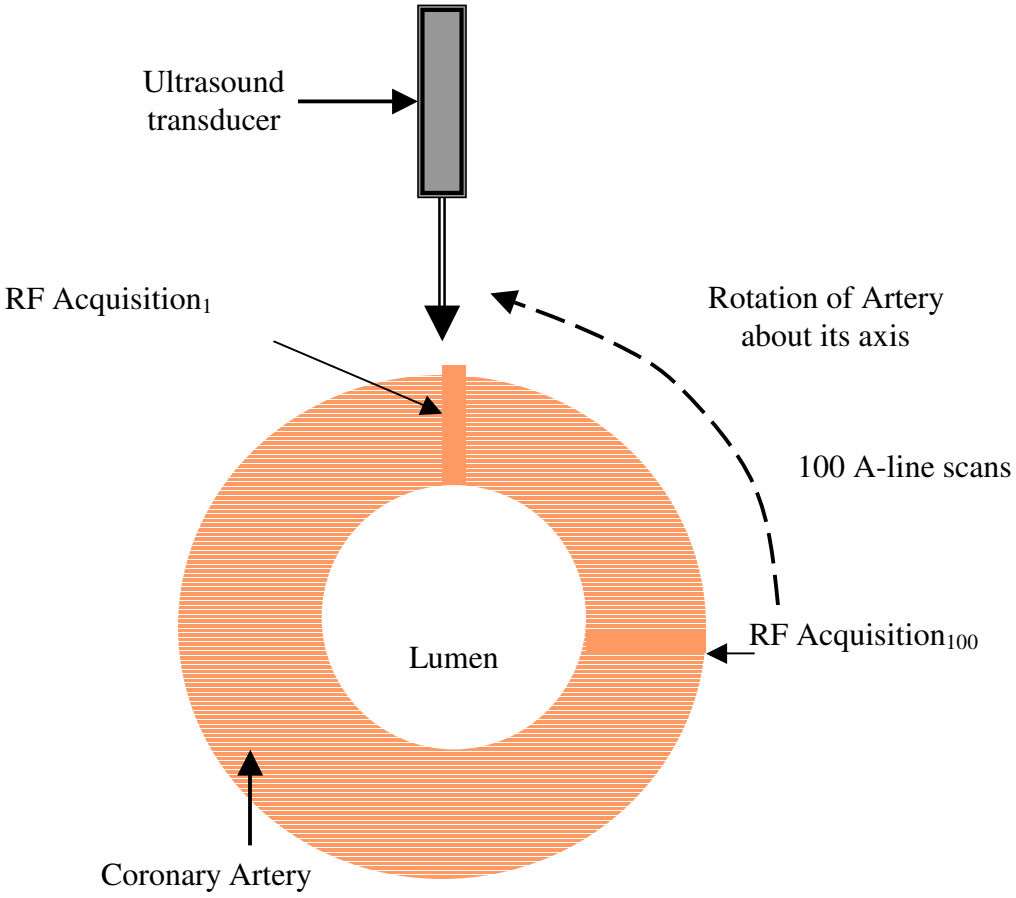

Figure 22: RF Data acquisition by rotating coronary artery in organ culture system

RESULTS

Data Processing for B-mode image formation:

The Hilbert transform is a relative of the Fourier Transform. It has several uses, one of which is to determine the analytic signal. The Hilbert transform has the property that all cosines are transformed to negative sines and all sine components are transformed into cosines [25]. The analytic signal of a real valued function f(t) is f(t) - i F(t), i is the complex number and F(t) is the Hilbert transform of f(t). The absolute value of the analytic signal gives us the envelope of the original function [10,25]. The received signals are high frequency, amplitude modulated signals. In order to make an image that does not contain this high frequency carrier wave, we need a way to only display the amplitude modulation.

The RF data was converted to image format using the absolute value of Hilbert transform (envelope detection method). Figure 23 shows the 50-MHz ultrasound image of the proximal wall of a fresh porcine artery. As the ultrasound wave propagates through the coronary tissue, it experiences inhomogenities causing reflection in form of pulses. The envelope detection method results in image formation from reflections in vascular tissue.

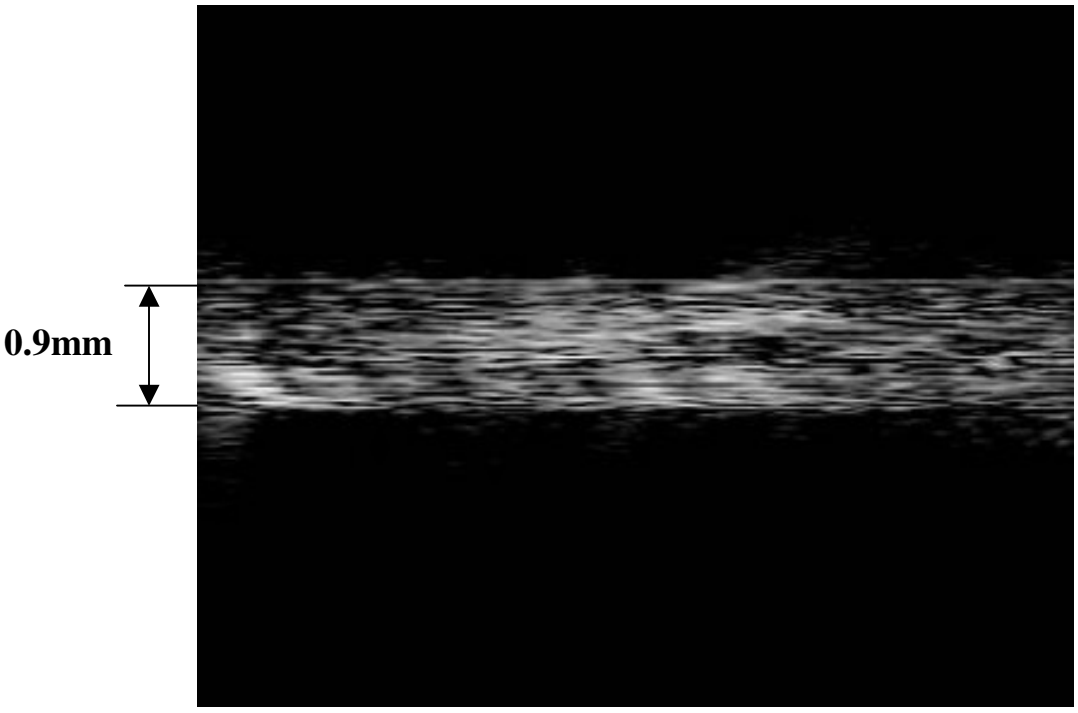

Figure 23: 50-MHz ultrasound image of the proximal wall of a porcine coronary

Compression Modulus of fresh porcine coronary artery:

Average strain values are calculated using elastography measurements. A set of precompression and postcompression waveforms for considered at a time [19,21,26,27]. The system noise was ereduced as described before. Successive windows were divided with 50% overlap [27] to determine the local time shifts between RF signals acquired at difference pressures. The time shifts were determined using the peak of the correlation function. The corelation function was upsampled by a factor of 100 [27]. Local radial strain ε was estimated using a one-dimensional finite difference algorithm [19,27]

The applied stress used in these experiments was 20mmHg, which corresponded 2.66kPa. Using the relation,

$$\sigma = E * \varepsilon \quad (8)$$

where σ is the applied stress, E is the compression modulus and ε is the strain [9], the compression modulus for different tissue types was calculated.

Table 2 shows the values of strain and compression modulus obtained from fresh porcine right coronary arteries.

Table 2: Value of strain and compression modulus of fresh porcine right coronary artery using elastography using elastography.

Sample	% Strain	Compression Modulus (kPa)
N1	0.84	316
N2	0.98	271
N3	1.03	255

The average value and mean deviation of the compression modulus is 281.11 ± 31.89

Compression modulus of fixed porcine coronary arteries

Values computed from arteries affected by 2% Glutaraldehyde for 30-35 minutes are as show in Table 3.

Table 3: Value of strain and compression modulus of porcine right coronary artery affected by 2% Glutaraldehyde for 30-35 minutes using elastography.

Sample	% Strain	Compression Modulus (kPa)
N4	0.49	535
N5	0.52	513
N6	0.45	589

Values computed from arteries affected by 3% Glutaraldehyde for 50-55 minutes are as show in table 4.

Table 4: Value of strain and compression modulus of porcine right coronary artery affected by 3% Glutaraldehyde for 50-55 minutes using elastography.

Sample	% Strain	Compression Modulus (kPa)
N7	0.34	794.02
N8	0.28	939.92
N9	0.31	844.4

In summary,

Table 5: Comparison of effect of Glutaraldehyde on properties of porcine coronary artery measured using elastography.

Sample	Mean Compression Modulus (kPa)	Standard Deviation
Fresh Porcine Coronary	281.11	31.83
2% Glutaraldehyde for 30-35 minutes	546.23	39.15
3% Glutaraldehyde for 50-55 minutes	859.44	74.1

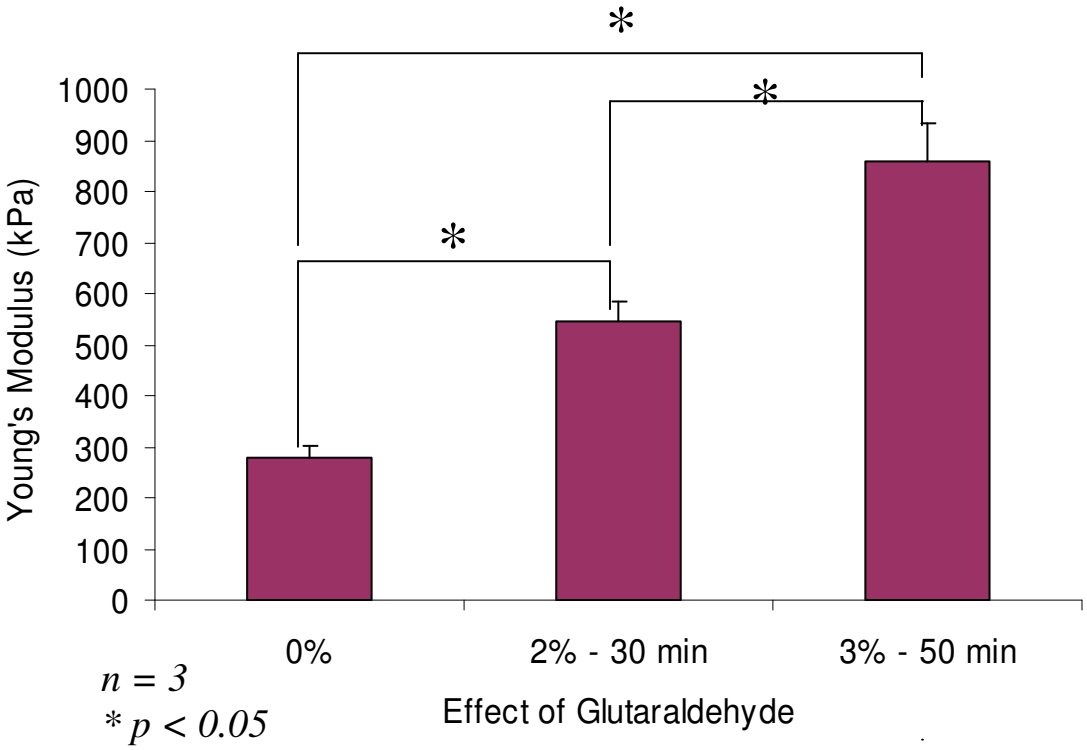

Figure 24: Young's modulus of porcine vessel walls measured by elastography

MECHANCIAL TESTING

Introduction

Tests used to determine the mechanical properties of biological tissues fall into three main categories: uniaxial tensile, biaxial tensile and biaxial or tri-axial pressurization. Uniaxial tensile tests are performed on strip specimens (Figure 24). Biaxial tests are performed on planar specimens (Figure 25). Pressurizing intact vessels while holding the vessel at a predetermined stretch performs biaxial and tri-axial pressurization tests; in tri-axial tests torsion is also applied [28].

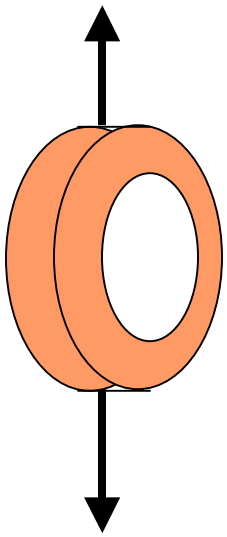

Figure 25: Uniaxial testing of ring specimens. Forces acting in one direction

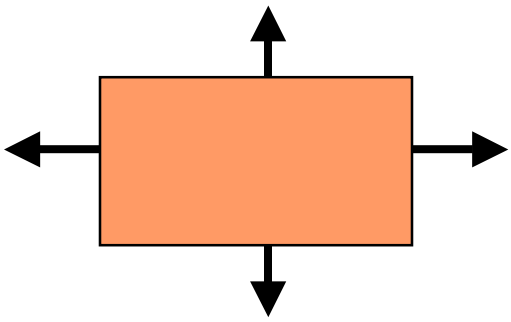

Figure 26: Biaxial testing of planar surface. Biaxial forces.

Uniaxial tensile tests are performed by gripping a strip of the excised vessel between the arms of a tensile tester (Figure 24) and recording the force and elongation [29,30,31]. Uniaxial tests can also be performed by pulling a ring specimen between two hooks [29,31,33]. One disadvantage is that uniaxial tests require the excision of a strip of the vessel, which not only disrupts the underlying structure, but also fails to yield the biaxial properties of the intact vessels [34,35].

Uniaxial testing results in calculation of various mechanical properties of tissue such as modulus of elasticity, which was sufficient to validate results from elastography of ultrasound A-line scans.

The specimen must be preconditioned before testing because the first few loading and unloading curves are usually not the same as successive curves [9,28]. Successive curves will have shifted from the initial curve such that the same load will produce a greater strain. Preconditioning consists of cycling the specimen between minimum and maximum values of force until a repeatable loading/unloading loop is obtained. This allows the structural components (smooth muscle, extra-cellular matrix etc.) to reorient to the load [28].

Procedure

The cuts for the mechanical testing were made with a razor at the points marked with dye at the same cross-section where ultrasonic data was acquired. The outer diameter, inner diameter and width were measured manually for each specimen with digital calipers. A disadvantage to this method of measurement is the possibility that forces applied to the specimen with the calipers caused errors in the measured values. In order to reduce the

amount of error, the measurements were taken in triplicate and averaged for use in calculations.

All of the specimens were tested on a servo-controlled electro-mechanical testing machine (Model 650 R, Test Resources, Shakopee, MN). This machine is used for universal mechanical testing applications such as tensile and compression testing. The system features a mechanical load frame and a load cell sized to produce loads to the user's test requirements. The maximum load capacity is 3kN [36]. To run the test, a load-controlled profile was created in the testing software (MTestWR). For the uniaxial test a load profile was setup. Once the profile (Figure 26) was set, the specimen was positioned onto two hooks. The hooks were securely placed into the grips of the machine in a position that placed no load on the specimen (Figure 25). This test was performed at room temperature (24ºC) and lasted between 10 and 30 s.

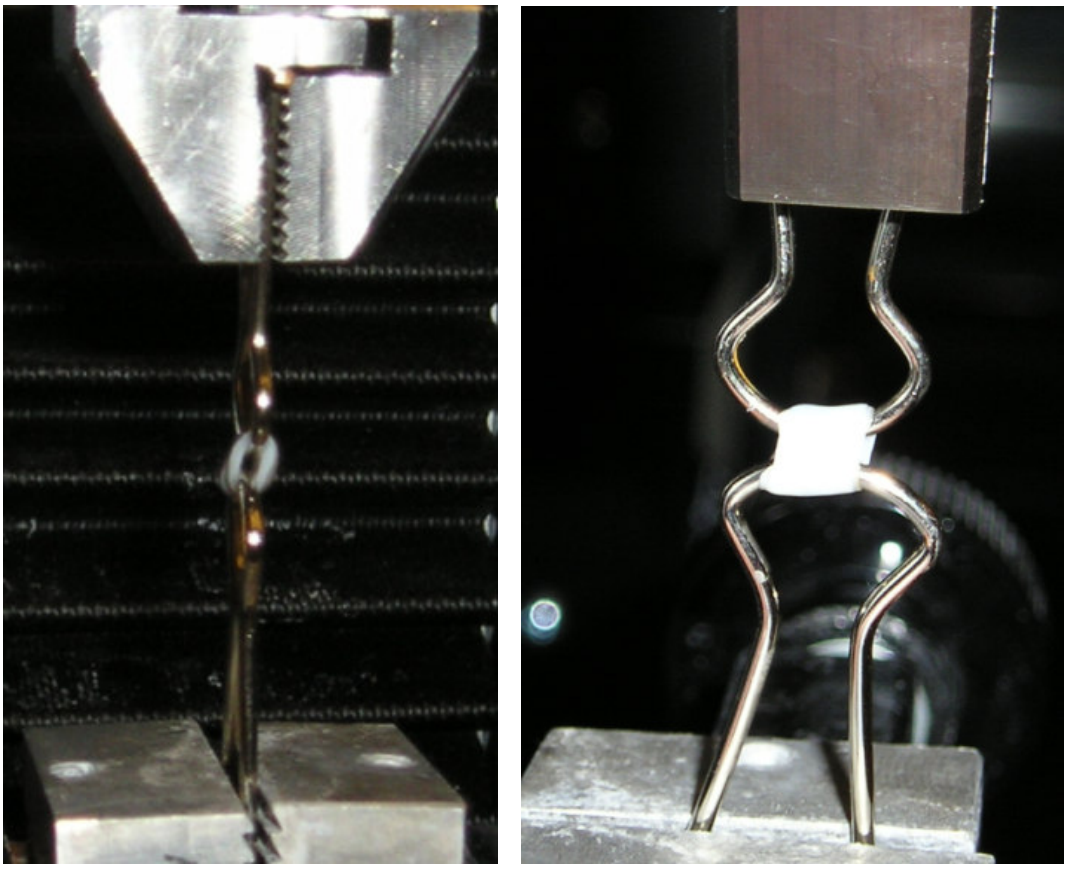

Figure 27: Illustration of mechanical ring testing of porcine right coronary artery

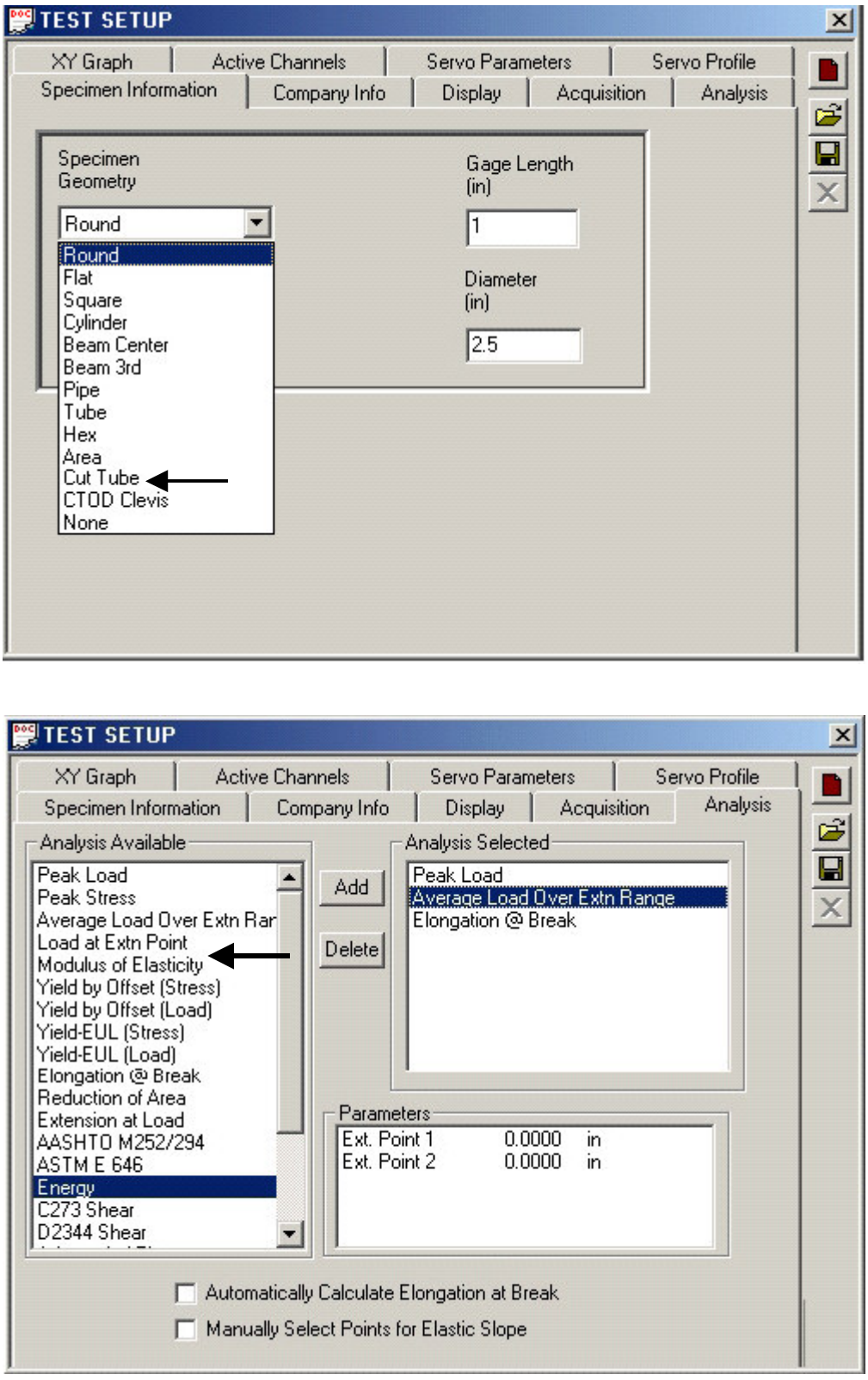

Figure 28: 650R Mechanical testing software (Test Resources, MN)

Results

The output of the mechanical testing was modulus of elasticity values. The machine calculates the modulus of elasticity value from the force and elongation measurements. The machine uses the differential area and the applied force to calculate the modulus of elasticity as follows.

The expression for stress S was the Kirchhoff's expression, obtained by dividing force F by the original unstressed area, A_0 of the specimen and by the stretch ratio λ [9,38]

$$S = \frac{F}{A_0\lambda} = \frac{F}{w_o t_o \lambda} = \frac{T}{\lambda} \qquad (9)$$

Where the strech ratio, $\lambda = \frac{l}{l_o} = l_o + \frac{\Delta l}{l_o}$ (10)

namely as ratio of length l of the specimen, corresponding to force F, to the original no-load length l_o, with Δl denotes the extension from unstressed state.

The expression for strain was in terms of longitudinal stretch ratio as follows [9,38],

$$E = \frac{1}{2}(\lambda^2 - 1) \qquad (11)$$

and the elastic modulus was calculated as the first derivative of stress S over strain E

$$M = \frac{dS}{dE} \qquad (12)$$

Table 6, 7 and 8 shows the Elastic Modulus values of the samples analyzed using ring test.

Table 6: Mechanical testing of fresh porcine coronary arteries using mechanical testing.

Sample	Compression Modulus (kPa)
N1	337
N2	278
N3	320

Table 7: Mechanical testing of fresh porcine coronary arteries fixed with a 2% Glutaraldehyde solution for 30-35 minutes using mechanical testing.

Sample	Compression Modulus (kPa)
N4	586
N5	538
N6	594

Table 8: Mechanical testing of fresh porcine coronary arteries fixed with a 3% Glutaraldehyde solution for 50-55 minutes using mechanical testing.

Sample	Compression Modulus (kPa)
N7	904
N8	927
N9	871

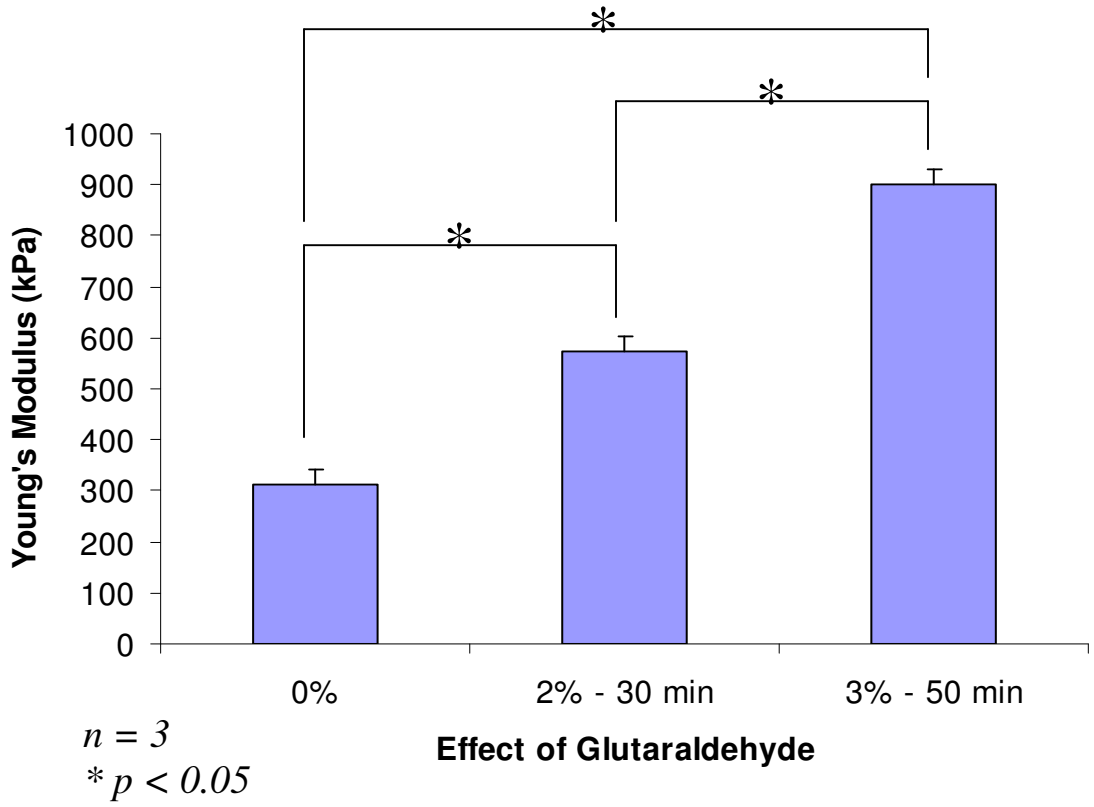

Figure 29: Young's modulus of porcine vessel walls measured by mechanical testing

In summary,

Table 9: Comparison of effect of Glutaraldehyde on properties of porcine coronary artery measured using mechanical testing.

Sample	Mean Compression Modulus (kPa)	Standard Deviation
Fresh Porcine Coronary	311	30.36
2% Glutaraldehyde for 30-35 minutes	572	30.28
3% Glutaraldehyde for 50-55 minutes	901	28.14

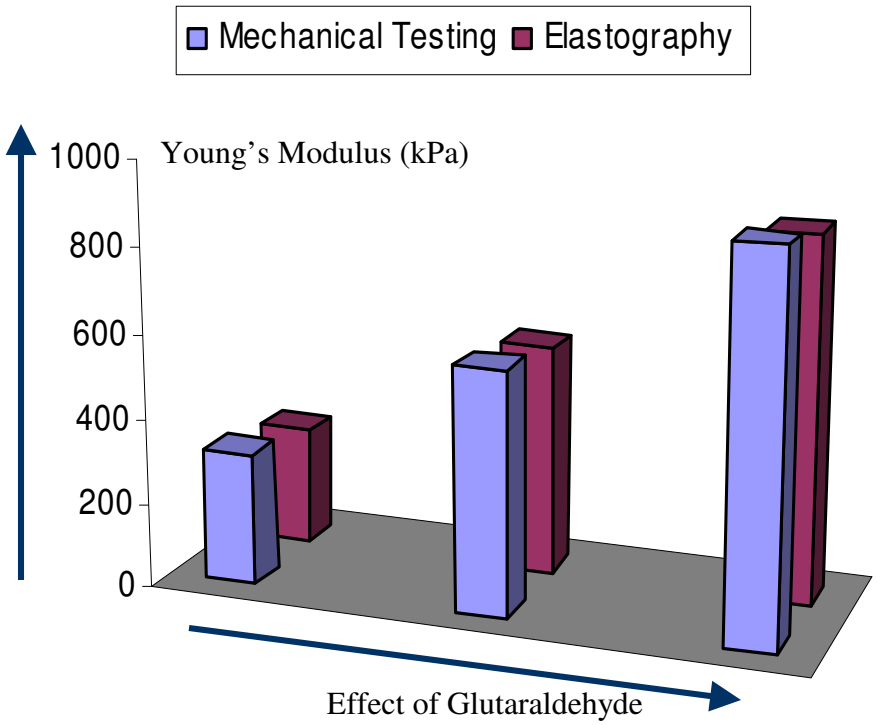

Figure 30: Comparison of Young's modulus of porcine vessel walls measured by elastography and mechanical testing

DISCUSSION

Quantitative comparison of compression moduli found in different studies is difficult, since the compression modulus is influenced by various measurements conditions (time after excision, temperature, effect of stretching) and each biological tissue even from the same species varies. Nevertheless, the compression modulus of normal vessel found in this study is in the same range as values found in literature for normal vascular tissue. Reported values range from 300 – 700 kPa [39,40,41].

Measurements of compression modulus using elastography in literature have yielded similar results [43,44]. The fibrous caps in atherosclerotic plaque have compression modulus values of 665 – 700 kPa [43,44]. There is a great similarity between mechanical values of human and porcine coronary arteries. The findings of the work done in this thesis are consistent with previous work done. This is the first time 50 MHz has been used to analyze coronary arteries using RF – elastography. Also a direct correlation was performed between mechanical testing and elastography for the first time ever.

Statistical Significance

Since there is high variability in values of elastic modulus in general [39,40,41], a one-sample t test was used to compare the mean of mechanical testing result with results from elastography. This aim of the thesis was to design and built a system capable of measuring a range of values of compression modulus. Statistical tests were performed to show that measurements of compression modulus made of samples affected with Glutaraldehyde were different from values measured with fresh porcine samples, hence

concluding that different compression modulus could be measured using Elastography. For all combinations $p < 0.05$ (Appendix), i.e., statistically significant.

Paired t-test is used for testing the difference between two means when the data are paired and the paired differences follow a normal distribution. A confidence interval of 95% was used in the analysis. The data from each sample must be in separate numeric columns of equal length. Each row contains the paired measurements for observation mechanical testing and elastography measurement. The difference was considered significant if p-value < 0.05.

Conclusion

The work in this thesis has successfully shown a technique to discriminate between various tissue types based on their mechanical properties. It is suggested to do more experiments on heterogeneous vessel mimicking phantoms or atherosclerotic human coronary arteries. Future work can include discriminating fibrous cap (compression modulus ~ 500 – 900 kPa) from fatty portion in plaques (compression modulus ~ 200 – 300) [43].

Result involving complete scanning of arteries would take a considerable amount of time as time required for pressure to change is a time consuming procedure (15 – 20 seconds); the whole process could take more than 5 hours. It is recommended to acquire a set of data at one pressure and another set of data at a different pressure and develop angle-matching algorithm to alleviate this issue. Human coronary arteries studies can be done, which will test elastography technique for heterogeneous tissue types. Moving target can be analyzed without changing the technique because signal discrimination method followed in this technique does account for motion artifacts.

Appendix A

VALPEY FISHER VF 412 TRANSDUCER. REFLECTION FROM GLASS SURFACE.

Transducer:	Valpey Fisher 50Mhz transducer
Frequency:	50Mhz
C:	1540m/s
Lambda:	0.0308mm
f-number:	focal length/element diameter = 2.5
Element Diameter:	0.2 inches
Focal Length:	0.5 inches
Pulse Width:	2 x 50ns = 100ns

Beam Diameter(-6dB): (1.02 x focal length x speed) / (frequency x element diameter) = 7.854 e-05 m = 0.07854mm

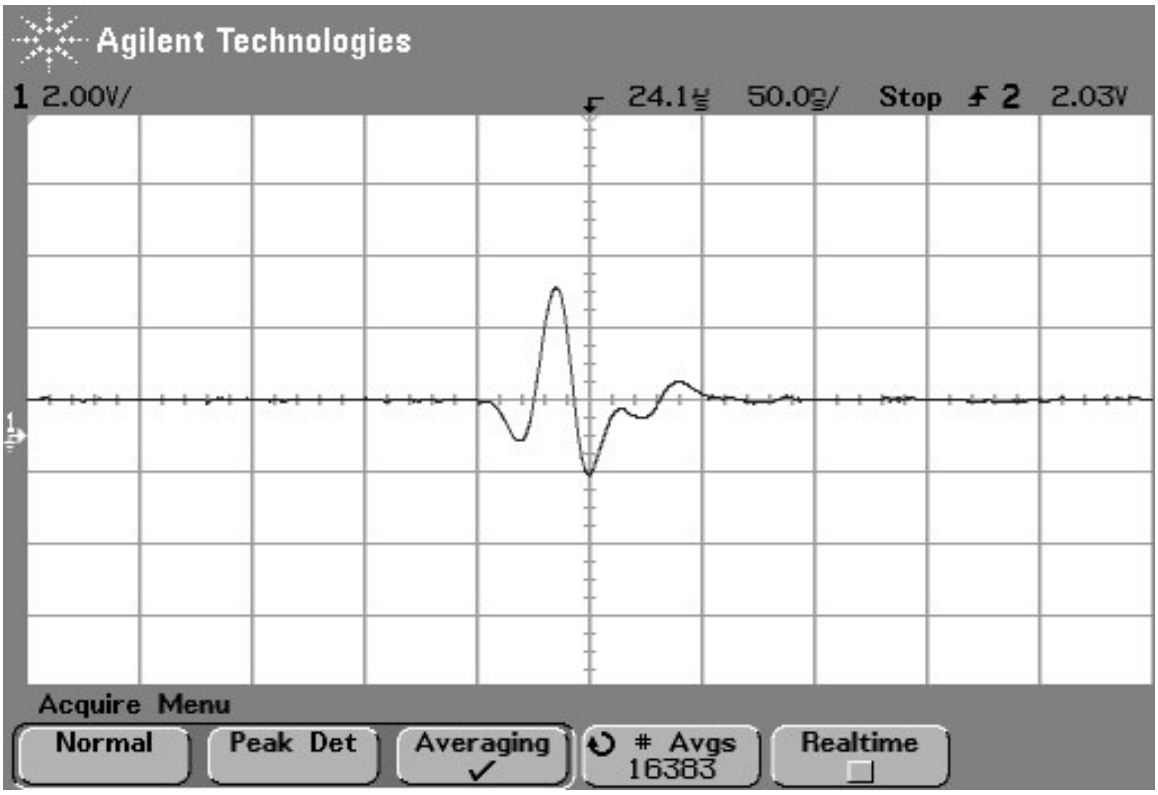

Appendix B

Algorithm for Strain Estimation of pressurized RF waveforms

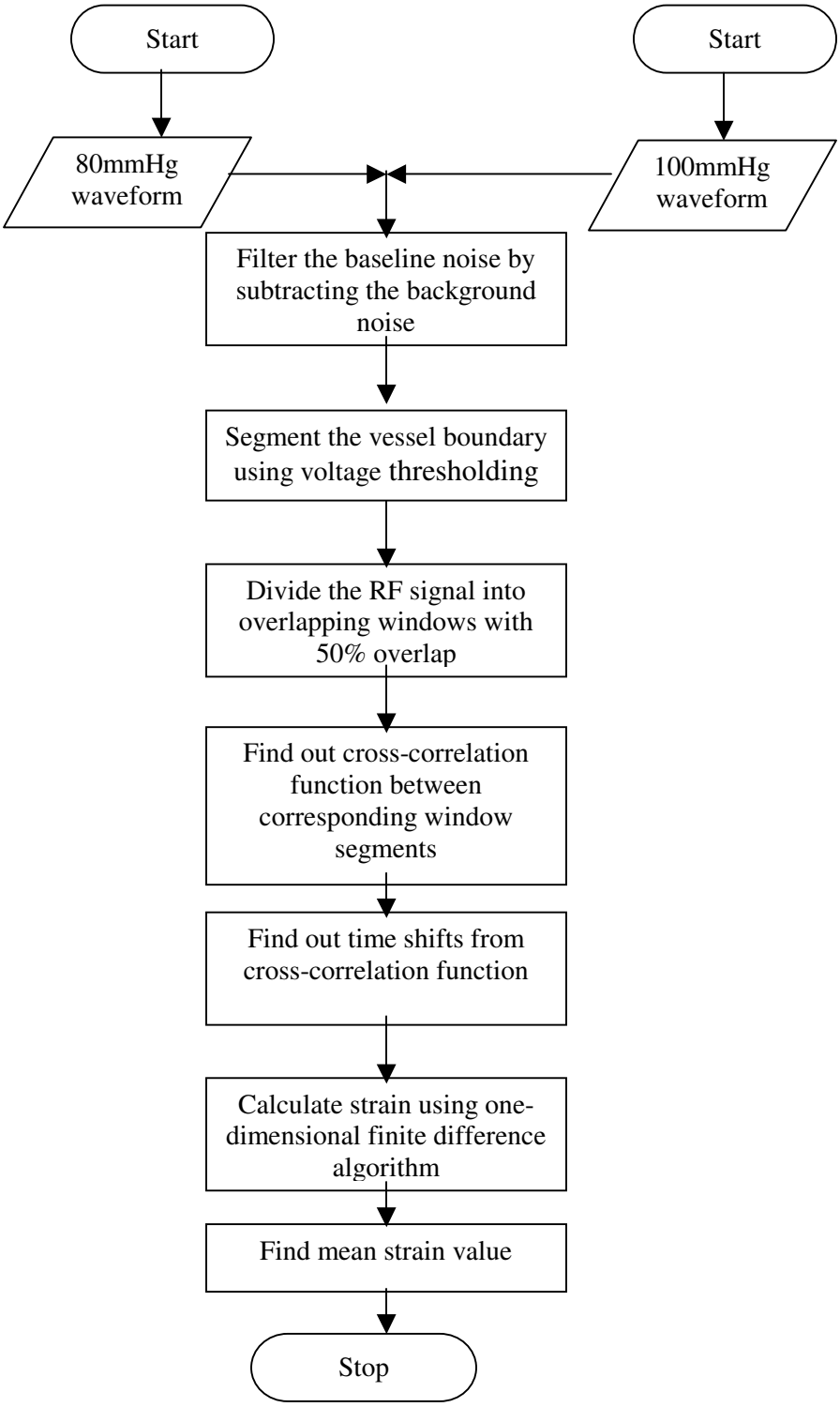

Appendix C

MATLAB Code for strain computation from pre and post compression RF Waveforms

```
%Strain Measurement

clear all; clc;
% This program measures strain using pressurized ultrasound RF waves


%data post fixed May 18 no gluta angle 7

x = load('blank.txt');
x1 = load('Waveform80.txt');
x2 = load('Waveform100.txt');
%

x3 = x1 - x;   % Subtracting the background signal from acquired signal
x4 = x2 - x;   % Subtracting the background signal from acquired signal
% subplot(3,1,1);plot(x);
% grid on;
% subplot(3,1,2);plot(x1);
% grid on;
% subplot(3,1,3);plot(x2);grid on;
% figure;


Ylim([-1.5 1.5])%Limiting the Y axis to have uniform display
subplot(2,1,1); plot(x3);grid on; title('RF Waveform at 80 mmHg');
xlabel('time/distance'); ylabel('amplitude/attenuation');
Ylim([-1.5 1.5])
subplot(2,1,2); plot(x4);grid on;title('RF Waveform at 100
mmHg');xlabel('time/distance'); ylabel('amplitude/attenuation');
Ylim([-1.5 1.5])

figure;


a2 = x3;%renaming the waveforms
b2 = x4;

% separating signal from the baseline noise by manually segmenting based on
% voltage values..An automated program can be designed for the same.
```

```
a2(1:800) = 0;
b2(1:800) = 0;
a2(1450:2000) = 0;
b2(1450:2000) = 0;


%STEP3: Divide the waveform into overlapping windows;
%strain distribution over the vessel wall..50% overlap

      a2set = buffer(a2,50,25);
      b2set = buffer(b2,50,25);


%STEP4: Crosscorrelation function


      for i = 1:80

        f(:,i) = xcorr(a2set(:,i),b2set(:,i));

      end


 %STEP5: Upsampling   (incresing resolution)


for i = 1:80
   temp = f(:,i);
   temp = interp(temp,100);
   fup(:,i) =  temp;
end

%STEP6: To find time shifts

for i = 1:80
   [q1,q2] = max(fup(:,i));
   p(i) = q2;
end

%Strain Estimate using one-dimensional finite difference algorithm
%Strain  = (dt2-dt1)/dT; dT = time between succesive window


for i = 1:79
```

```
    q(i) = (p(i+1) - p(i))/200000;
end

q = abs(q);

plot(q);grid on;
q4 = q(31:60);
mean(q4)
```

Appendix D

MATLAB Code for Image Formation

```
clear all;
clc;

%Image formation for RF signals


a = load('blank.txt');

a = a';


for i=1:120
   data(i,:)=dlmread(sprintf('trial%d.txt',i),'\t',1,0);
end

for i=1:120
   data(i,:)= data(i,:) - a;
end


for i=1:120
   data(i,:)= abs(hilbert(data(i,:)));
end

for i=1:120

   a = 0/0.0007128;
      for j = 1:2000
         data(i,j)= data(i,j) * a;
       a = a + 0.0007128;
      end
end

theta = 0:0.9:107.2;
%theta = theta * pi / 180;

for i = 1:120
   datan(i,:) = cart2pol(theta(i),data(i,:));
end

imshow(data);
```

Appendix E

Statistical Tests

One sample *t* test between mean of measured elastography values of fresh porcine coronary arteries and 3 samples of coronary arteries fixed with 2% Glutaraldehyde for 30-35 minutes.

The hypothetical mean is 281.00
The actual mean is 545.67
The difference between these two values is 264.67
The 95% confidence interval of this difference:
From 165.79 to 363.54
t = 11.5169
df = 2
standard error of difference = 22.981

The two-tailed P value equals 0.0075 (Statistically Significant)

One sample *t* test between mean of measured elastography values of fresh porcine coronary arteries and 3 samples of coronary arteries fixed with 3% Glutaraldehyde for 50-55 minutes.

The hypothetical mean is 281.00
The actual mean is 859.33
The difference between these two values is 578.33
The 95% confidence interval of this difference:
From 394.02 to 762.65
t = 13.5004
df = 2
standard error of difference = 42.838

The two-tailed P value equals 0.0054 (Statistically Significant)

REFERENCES

[1] Aldons J. Lusis, *Atherosclerosis* Nature Vol 407, Insight Review Articles, 14 September 2000

[2] DU Silverthorn. Human Physiology: An Integrated Approach. Textbook. 2nd edition. Prentice Hall.2001.

[3] Giddens DP, Zarins CK, Glagov. *The role of fluid mechanics in the localization and detection of atherosclerosis.* Journal of Biomechanical Engineering. 1993 Nov; 115(4B): 588-94.

[4] Celermajer DS *Endothelial dysfunction: does it matter? Is it reversible?* Journal of American college of cardiology. 1997 Aug; 30(2): 325-33.

[5] Ionita CC; Xavier AR; Kirmani JF; Dash S; Divani AA; Qureshi AI *What proportion of stroke is not explained by classic risk factors?* Preventive Cardiology 2005 Winter;8(1): 41-6.

[6] Bhatia V, Bhatia R, Dhindsa S, Virk A *Vulnerable Plaques, Inflammation and Newer Imaging Modalities* Journal of Postgraduate Medicine 49(4): 361-368.

[7] Kolodgie, FD; Burke, Allen P; Farb, Andrew; Gold, Herman K.; Yuan, Junying; Narula, Jagat; Finn, Aloke V.; Virmani, Renu *The thin-cap fibroatheroma: a type of vulnerable plaque: The major precursor lesion to acute coronary syndromes.* Current Opinion in Cardiology. 16(5): 285-292, September 2001.

[8] Loree HM, Kamm RD, Stringfellow RG, Lee RT. Effects of fibrous cap thickness on peak circumferential stress in model atherosclerotic vessels. *Circ Res.* 1992;71:850-858.

[9] Y C Fung *Biomechanics: Circulation* Second Edition Springer 1996

[10] Douglas Christensen *Ultrasonic Bioinstrumentation* John Wiley & Sons 1988

[11] Foster FS, Obara H, Bloomfield T, Ryan LK, Harasiewicz KA, Berube LR, Rauth AM. *Principles and applications of ultrasound backscatter microscopy.* IEEE Trans. Ultrason. Ferrielec Freq Control 1993;40:607 –617

[12] Stuart Foster, Chares Pavlin, Kasia Harasiewicz, Donald Christopher, Daniel Turnbull *Advances in Ultrasound Microscopy.* Ultrasound in Med & Biol. Vol 26, No. 1, pp1-27, 2000

[13] Muthupillai R, Ehman RL. *Magnetic Resonance Elastography* Nature Medicine 1996 May;2(5):601-3.

[14] S.I. Ringleb, Q. Chen, A. Manduca, *Quantitative Shear Wave Magnetic Resonance Elastography: Comparison to a Dynamic Shear Material Test* Journal of Magnetic Resonance in Medicine. 2005 May; 53(5): 1197-201.

[15] J Rogowska, N A Patel, J G Fujimoto and M E Brezinski *Optical coherence tomographic elastography technique for measuring deformation and strain of atherosclerotic tissues.* Heart. 2004 May;90(5):556-62.

[16] D.D. Duncan, S.J. Kirkpatrick, *Processing algorithms for tracking speckle shifts in optical elastography of biological tissues* J. Biomed. Opt. 6(4), 418-426 (2001).

[17] Saada, S., 1983. *Elasticity theory and applications.* , Pergamon Press, New York.

[18] Carlier SG; de Korte CL; Brusseau E; Schaar JA; Serruys, PWJC; van der Steen AF *Imaging of Atherosclerosis. Elastography* Journal of Cardiovascular Risk. 2002 Oct;9(5):237-45.

[19] Ophir J, Alam SK, Garra B, Kallel F, Konofagou E, Krouskop, Varghese T Elastography: ultrasonic estimation and imaging of the elastic properties of tissues. Proc Inst Mech Eng [H]. 1999;213(3):203-33.

[20] Whittingham TA *New and future developments in ultrasonic imaging* British Journal of Radiolgy. 1997 Nov;70 Spec No:S119-32.

[21] Ophis J, Cespedes I, Ponnekanti H, Yazdi Y, Li X *Elastography: A quantitative method for imaging the elasticity of biological tissues* Ultrasonic Imaging 13, 111-134 (1991)

[22] S. Tawqeer Rashid, Henryk J. Salacinski, George Hamilton, Alexander M. Seifalian. *The use of animal models in developing the discipline of cardiovascular tissue engineering:a review.* Biomaterials 25 (2004) 1627–1637

[23] Kantor B, Ashai K, Holmes DR Schwartz RS *The experimental animal models for assessing treatment of restenosis.* Cardiovasc Radiat Med. 1999 Jan-Mar;1(1):48-54.

[24] Verdonw PD *Domestic pigs in the study of myocardial ischemia.* Eur Heart J. 1983 May;4 Suppl C:61-7.

[25] Bracewell RN *The Fourier Transform & Its Applications* McGraw-Hill Science/Engineering/Math; 3 edition (June 8, 1999)

[26] Ophir J, Kallel F, Varghese T, Bertand M, Cespedes I, Ponnekanti H *Elastography: A Systems Approch* The International Journal of Imaging Systems and Technology, John Wiley & Sons, Inc, Vol. 8, pp. 89-103, 1997.

[27] de Korte CL, van der Steen AF, Cespedes EI, Pasterkamp G *Intravascular ultrasound elastography in human arteries: initial experience in vitro*

[28] Stacey Dixon *Biomechanical analysis of coronary arteries using a complementary energy model and designed experiments.* Thesis 2000 Mechanical Engineering; Georgia Institute of Technology

[29] Herbert ST, Badylak SF, Geddes LA, Hillberry B, Lantz GC, Kokini K. *Elastic modulus of prepared canine jejunum, a new vascular graft material.* Annals of Biomedical Engineering. 1993 Nov-Dec;21(6):727-33.

[30] Kowligi RR, von Maltzahn WW, Eberhart *RC Fabrication and characterization of small-diameter vascular prostheses*. Journal of Biomedical materials research.1988 Dec;22(3 Suppl):245-56.

[31] How TV, Clarke RM. *The elastic properties of a polyurethane arterial prosthesis.* Biomechanics 1984;17(8):597-608.

[32] Hellener G, Cohn D, Marom G. *Elastic response of filament wound arterial prostheses under internal pressure*. Biomaterials. 1994 Nov;15(14):1115-21.

[33] Hayashi K, Takamizawa K, Saito T, Kira K, Hiramatsu K, Kondo K. *Elastic properties and strength of a novel small-diameter, compliant polyurethane vascular graft.* Journal of Biomedical materials research. 1989 Aug;23(A2 Suppl):229-44.

[34] Brossollet LJ. *Mechanical issues in vascular grafting: a review*. International Journal of Artifical Organs. 1992 Oct;15(10):579-84.

[35] Silver FH, Christiansen DL, Buntin CM. *Mechanical properties of the aorta: a review*. Crtical Reviews in Biomedical Engineering

[36] Users manual 650T Test Resources (Shakopee, MN)

[38] Dimitrios P. Sokolisa, Harisios Boudoulas, Panayotis E. Karayannacos *Assessment of the aortic stress–strain relation in uniaxial tension* Journal of Biomechanics 35 (2002) 1213–1223

[39] Dixon SA, Vito RP, Heikes RG *Constitutive modeling of porcine coronary arteries using designed experiments*. Journal of Biomechanical Engineering.2003; 125:page 274-279

[40] Bergel DH *The static elastic properties of the arterial wall.* Journal of Physiology 1962; 156:445-457

[42] Gow BS, Taylor MG. *Measurement of viscoelastic properties of arteries in the living dog.* Circulatory Research 1968; 23:111-112

[43] de Korte CL, Pasterkamp G, van der Steen AF, Woutman HA, Bom N. *Characterization of plaque components with intravascular ultrasound elastography in human femoral and coronary arteries in vitro.* Circulation. 2000 Aug 8; 102(6):617-23.

[44] Hiroshi Kanai, PhD; Hideyuki Hasegawa, PhD; Masataka Ichiki, MD; Fumiaki Tezuka, MD; Yoshiro Koiwa, MD. *Elasticity Imaging of Atheroma with Transcutaneous Ultrasound. Circulation.* 2003;107:3018.